Macro-modelling approach for assessment of out-of-plane behavior of brick masonry infill walls

B. Pantò[1], L. Silva[2], G. Vasconcelos[2] and P.B. Lourenço[2]

1Department of Civil Engineering and Architecture, University of Catania, Italy

2 ISISE, Department of Civil Engineering, University of Minho, Guimarães, Portugal

Abstract

This paper deals with the numerical simulation of two solutions of brick infill walls developed at University of Minho under out-of-plane loading. The new solution of brick infills intend to represent an enhancement of the seismic performance of this constructive element. The numerical simulation is based on an innovative discrete macro-modelling strategy proposed by Caliò et al. (2014). This method is based on a hybrid approach by which the frame is modelled using concentrated plasticity beam-column elements, whereas the non-linear behaviour of masonry infill is modelled by means of a 3D discrete macro-element.

The main goals of this work are: (1) calibrate a numerical model based on the experimental results of the out-of-plane tests on two types of brick masonry infill walls; (2) assess the efficiency of the macro-modelling approach by comparing the numerical results; (3) assess the main influencing material and geometric parameters in the out-of-plane behavior of brick infill walls.

The results of the numerical simulation enabled to assess the good performance of the macro-modelling approach in simulating the seismic response of brick infill walls and predicting the failure mechanisms. In addition, it was possible to identify the main influencing parameters in the out-of-plane behavior of brick infill walls.

Keywords: Brick infill wall, numerical simulation, macro-modelling approach, parametric study

1 Introduction

The out-of-plane response of infilled frames due to earthquake actions was under scrutiny of different researchers to find out the main influencing parameters. The relevance of studying the out-of-plane behavior of brick infill walls was brought to light in the recent earthquakes occurred in Europe such as L'Aquila earthquake in 2009 (Braga et al. ,2011), where severe damages developed in the infill walls in comparison to some minor cracks observed in the surrounding structure. It was observed that no immediate occupancy was possible due to the generalized damage in the masonry infills. From several examples, it was seen that the ground motion was not strong enough to cause structural damage but due to improper anchorage and interaction of the infill walls with surrounding frame, the exterior walls tore away and the concrete beam and columns were exposed. In spite of the out-of-plane behavior of masonry infilled frames have attracted less attention from the research community than masonry infill under in-plane loading, some studies on the out-of-plane behavior of masonry infilled rc frames can be found in literature (Drysdale and Essawy,1988; Chuang et al., 2010; Flanagan and Bennett, 1999).

Experimental studies have been presented in literature in order to investigate the non-linear response of unreinforced masonry infills surrounded by reinforced concrete frames, subjected to actions orthogonal to their own plane. These tests have been performed by applying monotonic and cyclic uniform static loads to the infill, in order to simulate the effects of the inertia forces (Angel et al., 1994, Furtado et al., 2016, Akhoundi et al., 2016) or applying dynamic excitations (Tu et al., 2010).

A detailed numerical simulations of the out-of-plane response of infill frames requires computational expensive nonlinear finite element models, able to predict the damage on the masonry infill and the complex non-linear infill-frame interaction (Madan et al., 1997; D'Ayala et al., 1997; Singh et al., 1998; Asteris, 2008; Macorini and Izzuddin, 2011). However, these rigorous models are often unsuitable for practical applications due to its huge computational cost. With the aim to develop operative tools, capable of simulating the collapse mechanisms of large structures with a sufficient approximation, many authors have developed simplified methodologies (macro-models). They try to predict the global structural behaviour without obtaining a detailed representation of the non-linear local behavior of the material. The most used macro-model practical approach is the 'diagonal strut model', where the infilled masonry is replaced by a single unidirectional bar. Since its original formulations, in which only the in-plane behaviour of the infill was considered, this approach has been extended in order to include the out-of-plane behaviour (Furtado, 2016; Asteris et al., 2017; Di Trapani et al., 2017).

Following the need to have safer masonry infills, two solutions of brick masonry infill walls were developed at University of Minho. After the validation of the experimental behavior of both types of masonry infill walls under in-plane and out-of-plane loading, it was decided to calibrate a numerical model based on macro-modelling approach to describe the out-of-plane behavior. In this paper, the influence of the in-plane damage on the out-of-plane response of IFS is neglected. However, the latter is a key aspect in order to fully understand and simulate the response of real structures subjected to earthquake actions, as demonstrated by experimental (Angel et al., 1994; Oliaee and Magenes, 2016; Ricci et al., 2018) and numerical (Di Trapani et al., 2017) studies. Therefore, further investigations will be needed to complete the results here presented, including combined in-plane and out-of-plane loading scenarios.

In this work, an innovative 2D discrete macro-modelling strategy, proposed by (Caliò et al. ,2014), is employed. This method is based on a hybrid approach by which the frame is modelled using concentrated plasticity beam-column elements, whereas the non-linear behaviour of masonry infill is modelled by means of a 3D discrete macro-element, introduced and validated in Pantò et al. (2017). The non-linear interaction between the masonry infill and the surrounding frame is modelled by a 3D discrete non-linear interface elements, able to simulate the in-plane and out-of-plane flexural and sliding mechanisms (Pantò et al., 2018).

Therefore, the main goals of this work are: (1) to calibrate a numerical model based on the experimental results of the out-of-plane tests on two types of brick masonry infill walls; (2) to assess the efficiency of the discrete macro-modelling approach by comparing the numerical results obtained with the macro-model with the results obtained by a meso-scale modeling approach; (3) to assess the main influencing material and geometric parameters in the out-of-plane behavior of brick infill walls.

This paper is organized in three main parts: (1) review of the main experimental results of the out-of-plane tests on the brick infill walls; (2) derivation of material properties, numerical simulation of the out-of-plane behavior of the brick infill walls and assessment of the efficiency of the macro-modelling approach; (3) parametric study to evaluate the influence of different parameters in the out-of-plane response of the brick infill walls.

2 Brief overview of the masonry infills constructive systems

As mentioned above, one the main objectives of the present paper is to use a macro-model approach to simulate the out-of-plane behavior of brick masonry infills that were recently developed in the scope a research project (Insysme Project, 2017). These brick infills intend to result in a better behavior under seismic loading when compared to the traditional ones.

The first solution for masonry infill walls is called Uniko System (*System-1*). This system is a single-leaf masonry wall, with 100mm thickness, composed of a vertical perforated clay unit, see Figure 1. This unit has a tongue and groove system along the perforation direction. The masonry units are laid aligned in the vertical direction creating a continuous vertical interlocking joint, see Figure 1a. This intends to take advantage of sliding between masonry units, improving possibly the energy dissipation ability of the masonry infill. With this arrangement, it is intended that masonry infill can withstand inter-storey drift without damage for lateral drift for which traditional infills are already damaged. Aiming at enhancing the out-of-plane behaviour of the brick infill, it was decided to add steel rebars in the external recesses at the external faces of masonry units. These steel bars should be connected at top and bottom reinforced concrete beams. The masonry infill has dry vertical joints and mortared bed joints, for which a general-purpose M10 mortar is recommended.

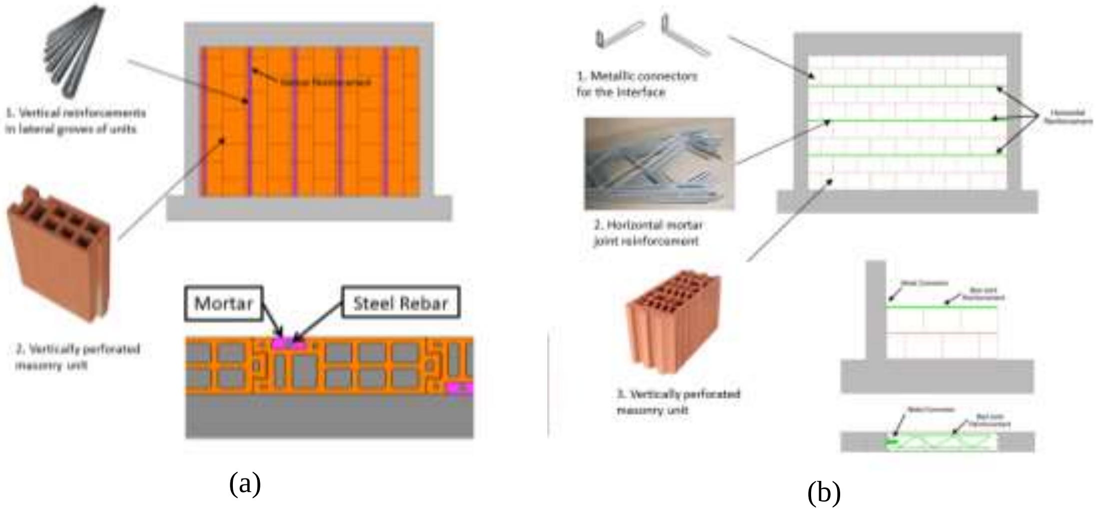

Figure 1 – Masonry infill systems: (a) System1, (b) System2

The second solution (*System2)* is called Térmico system, use the concept of maintaining the infill rigidly attached to the frame, using internal reinforcement and connectors between the infill and frame. This system is composed of a single-leaf clay masonry wall made with a commercial vertical perforated masonry unit produced in Portugal, see Figure 1b. The proposed system recommends a M10 mortar for the bed joints and dry head joint with interlocking. To improve the in-plane and out-of-plane performance of masonry infill walls, truss reinforcements was used in the bed joints. Additionally, the walls are connected to the columns by metallic connectors at each two rows where bed joint reinforcement is applied (see Figure 1b). The masonry infill panel was built with 294x187x140mm bricks with vertical perforation, using murfor RND 0.5 100 reinforcement and in each two rows, and murfor L +100 anchors to connect the infill and RC frame at the same levels of reinforcements.

The idea in Térmico system is making the infill and the frame one system, increasing the initial stiffness by using connectors and reinforcement, which not only helps to increase the maximum load, as to control cracking and the out-of-plane collapse.

3 An overview of the experimental Infill Frame Prototype out-of-plane behaviour

One of the steps of the validation of the two brick infill systems was the experimental testing under out-of-plane loading. For this, an experimental model was designed composed of a reinforced concrete (rc) frame (one bay, one storey) and a brick infill with one of the two solutions described previously. The reinforced concrete frame was built according to the actual building practice in Portugal. The dimensions of the prototype were defined based on an extensive work carried out on a database of buildings from different cities in Portugal: (a) rc frame was defined having a length of 4.50m and a height of 2.70m; (b) the cross section of rc columns was 0.3m x 0.3m (length x height) and (c) the cross section of rc beams was 0.3m x 0.5m. The reinforcing schemes were defined based on EC8 (NP EN 1998-1, 2010) recommendations. Due to the laboratory limitations, it was decided to test reduced scale specimens. For this, Cauchy's Similitude Law was considered (Akhoundi et al., 2018). Therefore, the geometry of the frame was reduced to 2/3 times of the prototype rc frame and the reinforcing scheme of columns and beams was updated in relation to the reinforcing schemes of the rc frame prototype, see Figure 2. The frame has 2735 mm in length and 2175 in height. The dimensions of beams and columns sections are 270×160 mm and 160×160 mm, respectively. The brick infills were built according to the details previously described. For each solution, a reinforced and a non-reinforced brick infill was considered so that the performance of the reinforcing schemes could be assessed.

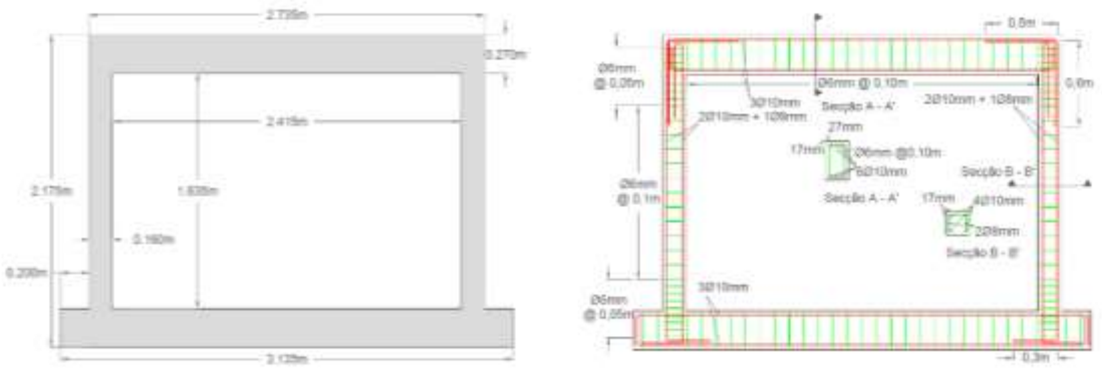

Figure 2 – Details and dimensions of experimental RC frame.

The rc frames with brick infill solutions were tested under out-of-plane loading according to the procedure pointed out by (Akhoundi, 2016). The out-of-plane loading was applied by means of an airbag that was connected to an external supporting frame. The time cyclic load history used in the out-of-plane tests was adapted from the procedure recommended in (FEMA 461, 2007) for in-plane. It consists of a cyclic procedure composed of two cycles of load and unloading for increasing levels of out-of-plane displacement. The increments of displacement at each two cycles *i+1* is about 1.4

times the displacement corresponding to the previous two cycles *i*. The out-of-plane test was carried out under displacement control by imposing the load displacement history at the central point of the brick infill (mid span and mid height). The loading was performed in one direction to monitor the deformation of the infill, propagation of cracks and assessment of the separation of the brick infill in relation to the rc frame.

The monotonic envelops of the experimental cyclical responses of the brick walls (reinforced and unreinforced) are presented in Figure 3 With reference to the first (continuous line) and second cycle (dashed line).

The maximum resistance obtained in the unreinforced Sistem1 wall (US1) was equal to 52.50kN, corresponding to a lateral 20.01mm of displacement. The maximum displacement before collapse was 53mm (Figure 3a). The test stopped because of the collapse of infill, followed also by a reduction of resistance. The lateral resistance attained in the second cycle is very close to resistance recorded in the first cycle, particularly in the elastic range of the wall. After these first steps, it is possible to see a small reduction of lateral force in second cycle, being of approximately 7.1%. The addition of vertical steel bars to the brick infill with vertical continuous joints (US2) resulted in a significant increase of the out-of-plane resistance (Figure 3b).

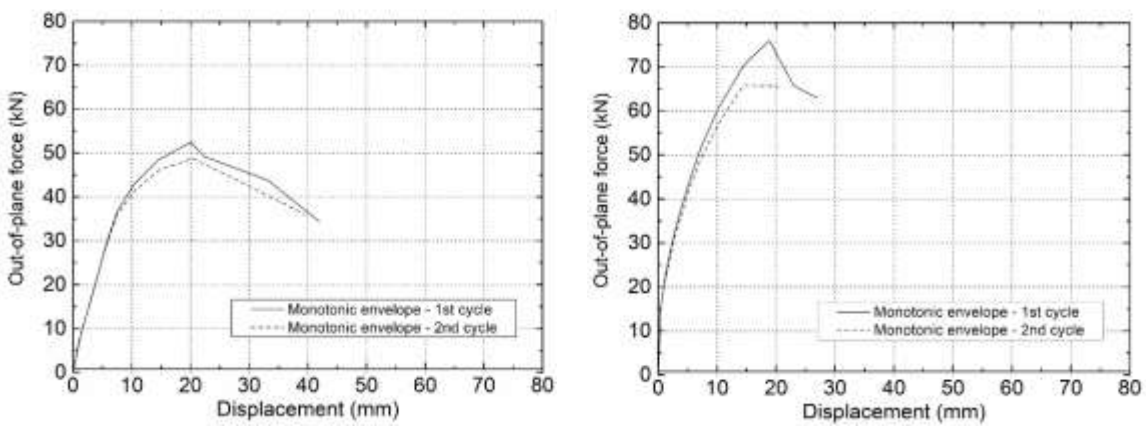

(a) (b)

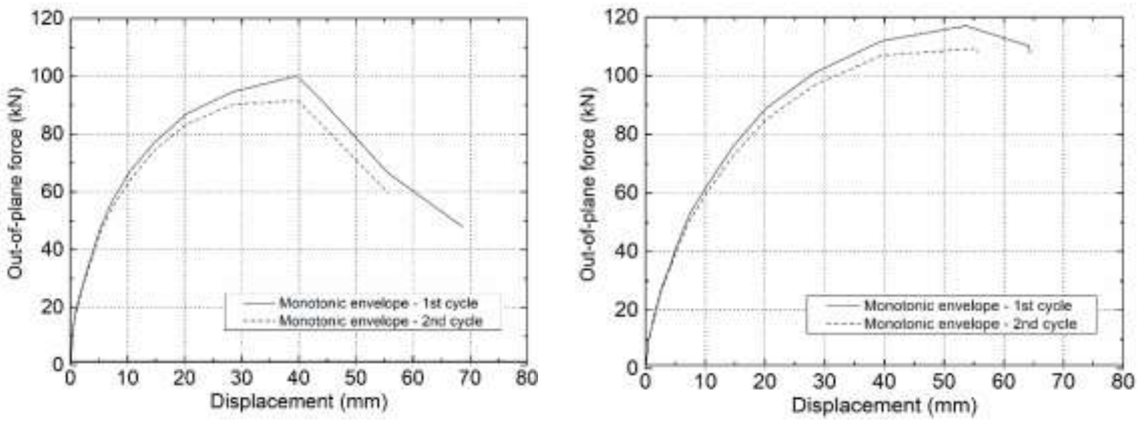

(c) (d)

Figure 3 - Load-displacement envelope curve for first and second loading cycle for; (a) solution 1 – non-reinforced (US1); (b) solution 1 reinforced (US2); (c) solution 2 –non-reinforced (TS1); (d) solution 2 – reinforced (TS2).

In this case, the maximum resistance was equal to 76kN for 18.81mm of displacement, representing an increment of 44,8% in comparison with the unreinforced wall.

The maximum displacement applied before collapse was around 27mm. The test stopped due to the localized collapse of infill in a vertical joint due to the failure of interlocking system. The force response during the second cycle is almost the same of first cycle until the cracking occurs. After this stage, there is a degradation of the lateral resistance in the second cycle of loading of about 13.6%.

In the case of brick infill system2, it is seen that the out-of-plane resistance of the unreinforced specimen (TS1) was 100.15kN, attained for an out-of-plane displacement of 39.67mm, see Figure 3c. The maximum displacement applied before collapse was 68.71mm. The test stopped due to the collapse of the infill. The out-of-plane force during the second cycle is almost the same of first cycle until the onset of cracking. After this stage, it is possible to see the reduction for second cycle. For the reinforced System2 brick masonry infill (TS2), an increase of about 16,9% of out-of-plane resistance was observed, see Figure 3d. For this masonry infill wall, the maximum resistance was equal to 117.05kN, achieved for a lateral displacement at the central point of the infill of about 53.6mm. The maximum displacement applied was around 64mm corresponding to a stage near to wall collapse. The test stopped because the imminent collapse of infill.

The presence of reinforcement changes the crack patterns observed in both types of brick infills, see Figure 4. The presence of reinforcement results in a more distributed crack pattern, particularly in case of system 1. In the unreinforced brick infill (US1) the cracks develop at mid height of the wall, mainly along the mortar bed joints. There is also a concentration of damage close to the columns characterized by crushing of some brick units. This crack pattern appears to be associated to a predominant one-way vertical bending. Conversely, the cracking developed in reinforced masonry infill is more associated to the development of two way bending. In spite of the cracks develop along the horizontal bed joints, they develop along the adjacent are of diagonal struts.

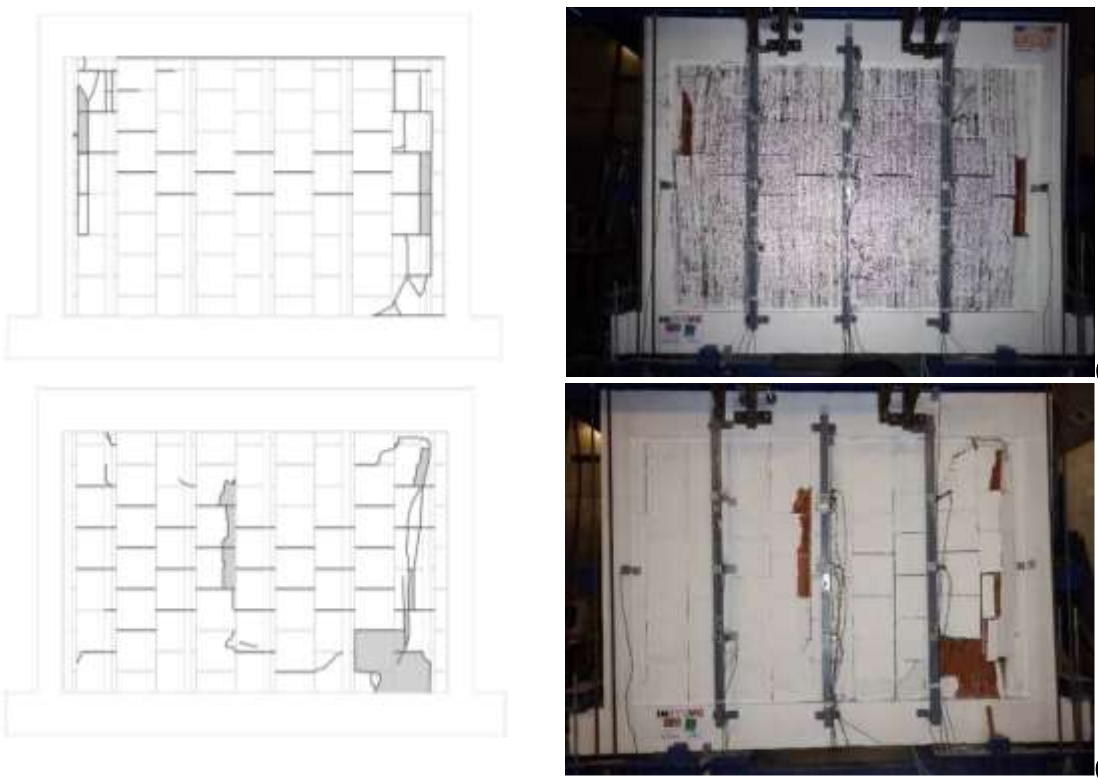

(a)

(b)

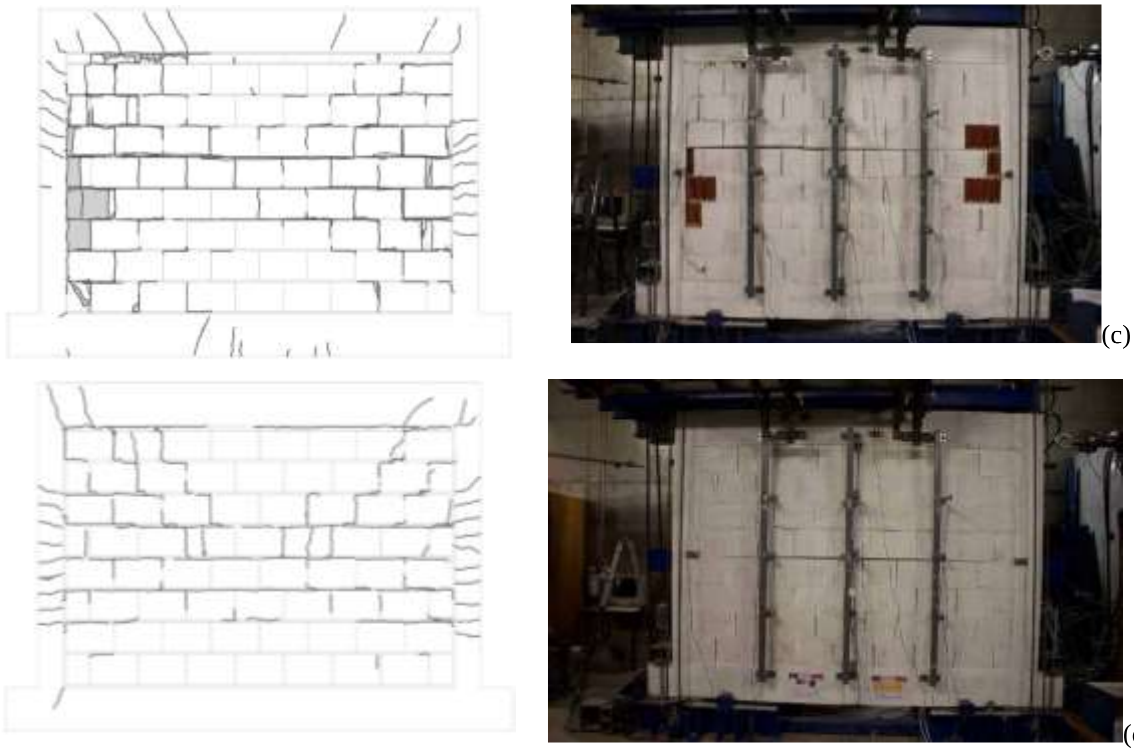

Figure 4 – (a) Cracking pattern of US01 at out-of-plane displacement of 53mm; (b) Cracking pattern of US02 at out-of-plane displacement of 26.98mm; (c) Cracking pattern of TS01 at out-of-plane displacement of 68.70mm; (d) Cracking pattern of TS02 at out-of-plane displacement (max disp.) of 64.37mm.

The cracking in the masonry infill with termico brick units starts along the central bed joint and progress along diagonals of the walls, which result from the development of two way bending mechanism. At the end of the test, crushing of the brick units close to the columns occur. In case of the reinforced brick infill, it appears that the two-way bending mechanism also develop, but the cracking is less severe. Besides, there is no signs of crushing of the brick units. This means that the addition of horizontal reinforcement and connectors allow a better control of damage in the infill wall for the same levels of displacement. In both cases, some microcracks develop in the rc frame, particularly in the columns. This should result from the much higher level of out-of-plane resistance of this type of infill and appears to demonstrate a higher interaction between the brick infill and the rc frame. It should be noticed that in case of System1 any cracks appears in the rc frame.

4 The Macro-modelling approach

In order to numerically simulate the experimental tests on the unreinforced and reinforced infill frame prototypes, an innovative discrete macro-modelling strategy, proposed by (Caliò et al., 2014), is employed. This method is based on a hybrid approach by which the frame is modelled using concentrated plasticity beam-column elements, while the non-linear behaviour of masonry infill is modelled by means of a 3D discrete macro-element, introduced and experimentally validated in (Pantò et al. ,2017). The model is able to simulate the axial-2D out-of-plane bending moment interaction on unreinforced masonry panels loaded orthogonally to own plane with different external bond conditions. The non-linear interaction between the frame and the infill is modelled by means of discrete non-linear interface elements which simulate the tensile cracking, the crush of the masonry and the sliding between masonry and frame. In order to take into account the complex out-of-plane interaction mechanisms between the infill and frame elements, a new 3D discrete interface was developed in (Pantò et al 2018).

4.1 The Discrete Macro Model (DMM) for masonry infills

The three-dimensional discrete element used to simulate the masonry is based on an innovative macro-element introduced by (Caliò et al. ,2012), originally developed to simulate the in-plane non-linear response of unreinforced masonry walls, later extended to the mixed concrete-masonry structures and infill frame structures (Caliò and Pantò, 2014). The extension of the existing model to a 3D kinematic model was introduced and numerically validated in (Pantò et al. ,2017). This model is represented by means of a simple *discrete* mechanical scheme consisting of an articulated quadrilateral (*panel*) with four rigid edges and a diagonal link, connected to the corners, to simulate the masonry shear behaviour (Figure 5a). Each side of the panel interacts with other panels, frame elements and or ground supports by means of a discrete distribution of nonlinear springs, denoted as *interface*. Each interface is constituted by a *m x n* grid of non-linear springs, orthogonal to the panel edge (Figure 5b). In addition, at the same interface, a longitudinal in-plane spring controls the relative sliding in the direction of the panel edge, whereas two longitudinal out-of-plane longitudinal springs control the out-plane sliding and the torsion behaviour (Figure 5c).

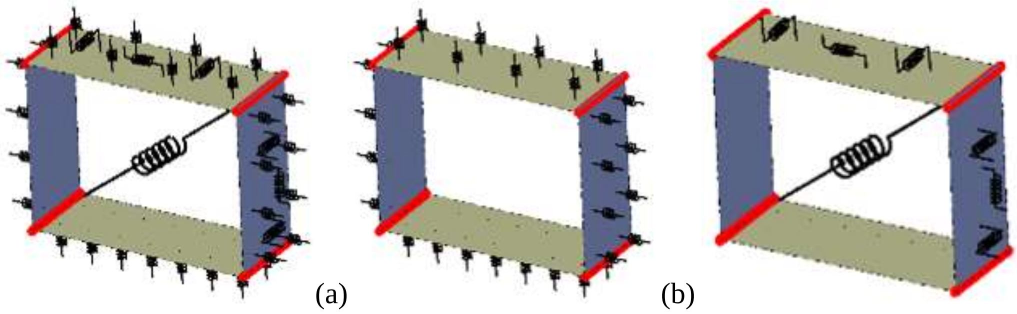

(a) (b) (c)

Figure 5 - Discrete macro-element: (a) mechanical scheme; (b) representation of the orthogonal springs; (c) representation of the longitudinal in-plane and out-of-plane springs.

The kinematic of this spatial macro-element is governed by seven degrees of freedom, able to describe the rigid body motions and the in-plane shear deformability of the panel. The calibration procedures of each non-linear link material properties are based on simple mechanical equivalences imposed between the discrete macro-model and the equivalent continuous homogenised models.

The orthogonal links of the interfaces intend to describe the flexural/axial behaviour of the masonry which is assumed as an orthotropic homogeneous media material. Each link inherits the nonlinear behaviour of the corresponding fibre along each main direction of the material (see Figure 6a). Each spring is calibrated assuming that the masonry strip is a homogeneous elasto-plastic material, according to the procedure reported in (Caliò et al., 2012) and (Pantò et al., 2017). A linear softening behaviour governs the post-yielding response under tension and compression, ruled by fracture energy values in tension (g_t) and compression (g_c), to which the corresponding ultimate displacements u_t and u_c are associated, see Figure 6b.

The shear in-plane and out-of-plane springs are modelled respectively by means of a rigid and an elasto-plastic constitutive law governed by the Mohr–Coulomb yielding surface. A linear relationship between stress and sliding describes the post-peak behavior governed by the shear fracture energy (g_s).

The capability of this model to simulate the structural behaviour until collapse has been validated by (Marques and Lourenço, 2014) and (Pantò et al., 2017) with reference to multi-storey mixed buildings and by (Pantò et al., 2016) with reference to monumental structures.

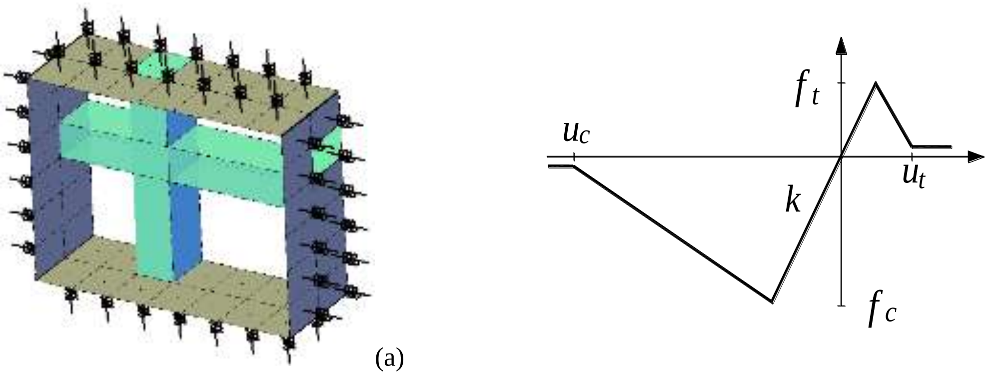

Figure 6 Definition of the material properties of orthogonal links **;** (a) Two generic orthogonal links and the corresponding fibre representations ; (b) constitutive law associated to the transversal springs.

4.2 The Modelling of the frame-masonry interaction

The frame elements interact with the masonry panels along the entire length by means of non-linear orthogonal links, uniformly distributed into contact with *infill-frame* interfaces. Each interface, as those between masonry panels, includes *n x m* orthogonal links, a single longitudinal in-plane non-linear link and two out-of-plane longitudinal links. In order to simplify comprehension, Figure 7a shows the in-plane degrees of freedom governing the in-plane panel-frame interaction, while Figures 7b 7c and 7d show the 3D mechanical scheme distinguishing flexural (Figure 7b), in-plane sliding (Figure 7c) and out-of-plane sliding interaction (Figure 7d). In the figures, the afference area associated to each link, obtained discretizing the transversal cross section of the panel, is also reported. The interface links are characterised by an elasto-plastic constitutive law with linear-softening branch, calibrated from the macroscopic mechanical properties of masonry and the afference volume of the link (Pantò et al., 2018). In particular, the flexural transversal links are characterized by the tensile and compression masonry strengths (f_t, f_c) and the corresponding fracture energies (g_t, g_c). The ultimate strength of the in-plane and out-of-plane sliding links is determined by the masonry cohesion (c) and friction factor (μ) through a Mohr-Coulomb domain. Finally, the ultimate capacity displacement of the sliding links is determined assigning the sliding fracture energy (g_{sl}). More details on the model kinematics and on the link calibration procedures can be found in (Pantò et al. 2018).

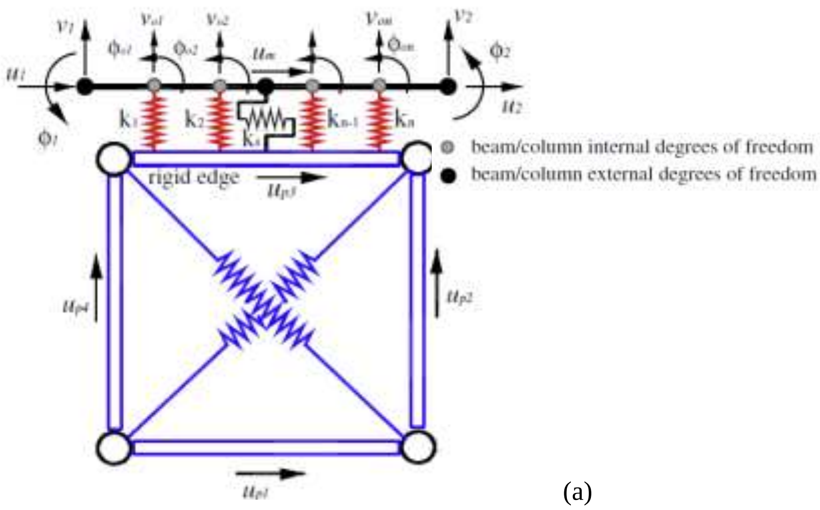

(a)

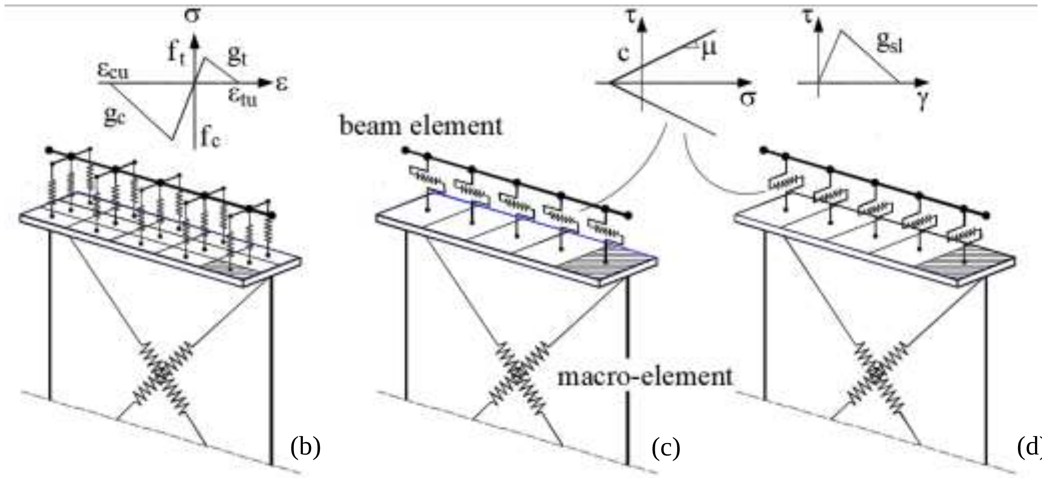

Figure 7 - Mechanical scheme of the in-plane masonry-frame interaction (a); mechanical scheme of the out-of-plane masonry-frame interaction: flexural (b), in-plane sliding (c) and out-of-plane sliding (d) interface links.

This macro-model is particularly appropriate to simulate the flexural and sliding forces shared between the frame and masonry panel providing a reliable prediction of the bending moment distribution on the frame (Caliò and Pantò, 2014). For the sake of clarity, in Figure 8 a simple structural prototype constituted by a full infilled regular brick-wall frame (Figure 8a) is modeled by a 3x3 mesh of macro-elements (Figure 8b). The ultimate frame bending moment corresponding to a horizontal in-plane force applied at the top beam (Caliò and Pantò, 2014), is reported in Figure 8c.

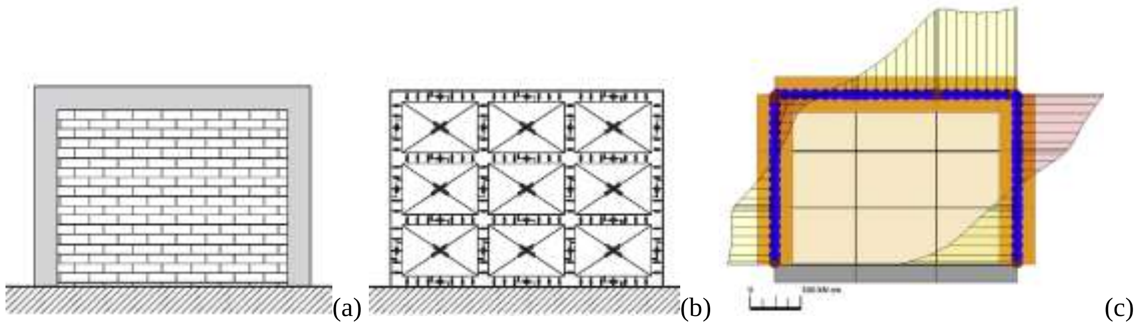

Figure 8 Infill frame structure: (a) typological geometrical scheme; (b) macro-modelling of the infilled frame by means of a 3x3 mesh of macro-elements; (c) typical bending moment prediction associated to horizontal actions.

4.3 ***2D macro-modelling approach versus the equivalent strut model***

In this section, the 2D Discrete Macro-Model is compared with the equivalent strut-model which represents one of the most used macro-model approach both for engineering and research purposes. In particular, a strut model formulation, recently proposed to simulate the in-plane and out-of-plane behaviour of IFS (Di Trapani et al., 2017), is considered. This model is composed of four struts: two diagonal struts plus two horizontal/vertical elements. Each strut consists of two fiber-section beam-column elements characterized by a rectangular section with in-plane width (*w*) and thickness (*t*). The mechanical behaviour of the fiber is characterized by the Kent and Park model (Kent and Park, 1971) assigning the peak (f_{m0}) and residual stress (f_{mu}) and the corresponding strain (ε_{m0}, ε_{mu}). More details on the calibration of the model can be found in (Di Trapani et al., 2017).

The two models are compared in terms of capacity curves considering the test-1 performed by Angel (Angel et al., 1994) on a single bay, one storey, infilled reinforced concrete frames with brick-clay masonry infill. The test was performed monotonically by applying a uniform out-of-plane pressure across the infill surface after applying the vertical loads consisting of two concentrated forces of 200 kN at the top section of each column.

The strut model is calibrated according to (Di Trapani et al., 2017) with reference to the test-2 of the Angel’s campaign, characterised by the same frame geometry and masonry typology of the tes-1, here considered. The geometric and mechanical parameters characterizing the struts are reported in Figure 9a. The analyses are performed in OpenSees (McKenna, 2011) using Force-Based Beam-Column Element (Taucer et al., 1991) both for the frame and the struts and considering 40x40 fiber-grid discretization for each cross section. The concrete is modelled by the Kent and Park model while the steel bars are modelled by the Menegotto and Pinto constitutive law (Menegotto and Pinto, 1973).

The numerical out-of-plane capacity curve obtained by means of the 2D macro-model is reported in (Pantò et al. 2018) and here shown in Figure 9b, compared with the results obtained by the strut model and the experimental findings. These capacity curves are expressed in terms of lateral displacement of the central point of the infill against the applied external force. Both models provide a satisfactory prediction of the experimental response. In particular, the two numerical curves are very close to each other in terms of initial stiffness and ultimate strength. In the non-linear pre-peak phase, the strut model and the 2D macro model tend respectively to overestimate and underestimate the experimental response. However, the differences between the two models are less than 15% and both lead to a very good prediction of the peak load (about 5% of error). Larger differences are observed in the post-peak phase where the 2D macro-model, coherently to the experiment, presents a softening behaviour not provided by the strut model.

Strut	w	t	f_{mo}	f_{mu}	ε_{mo}	ε_{mu}
	(mm)		(MPa)		(%)	
Diag.	203	230	2,25	1,35	0,15	0,80
Vert.	679	48	10,85	6,51	0,15	0,80
Horiz.	454	48				

(a)

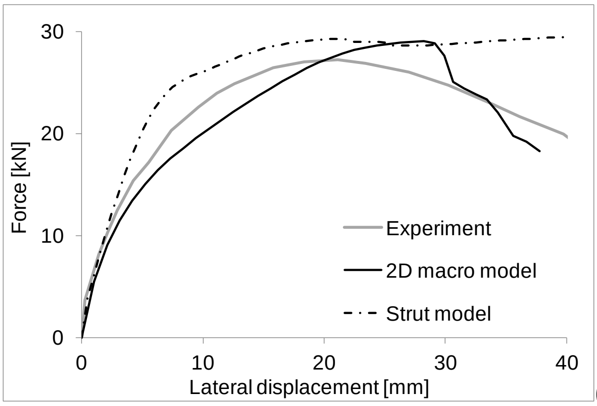

(b)

Figure 9 Mechanical calibration of the equivalent strut model (a); comparison between the experimental response and the numerical predictions of the two macro-models (b).

5 Simulation of the out-of-plane behaviour of the unreinforced prototypes

In this section, the discrete macro-model described in section 4 is employed to numerically simulate the experimental behaviour of the masonry brick infill solutions, previously described in section 2 (*system 1* and *system 2*). According to this modelling strategy, the orthotropic behaviour of the masonry material is taken into account by means of the calibration of the interface non-linear links. With this aim, two different one-dimensional constitutive laws are considered to characterize the masonry along the horizontal and vertical direction (or parallel and orthogonal directions to the bed joints). More details on these procedures can be found in (Pantò et al. ,2017). The numerical simulations aim at providing the capability of the macro-model in predicting lateral stiffness, ultimate strengths and failure mechanisms of the infill frame prototypes. The results of the numerical analyses and the comparisons with the experimental findings are reported and critically commented in the following.

A detailed mesh of macro-elements with size 15cm x 15cm is considered for both prototypes (Figure 10) in order to accurately simulate the out-of-plane behaviour of the infill panels and to obtain a high detailed representation of the collapse mechanism and plastic damage distribution. Each model is constituted by 150 macro-elements, corresponding to 1050 degrees of freedom, and by 35 beam elements, corresponding to 204 degrees of freedom (Figure 10).

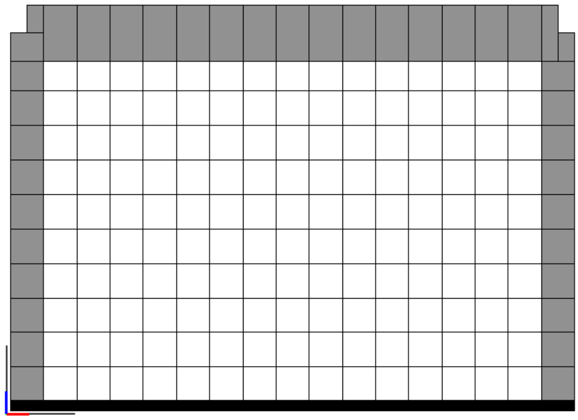

Figure 10 Mesh of discrete macro-elements

In order to evaluate the performance of the macro-model, in section 5.4 the results obtained by the latter model are compared with those obtained by a meso-scale modelling approach which enables a 3D representation of the effective brick arrangement of the two masonry systems. The comparisons are presented and critically discussed in terms of capacity curves and failure mechanisms.

The frame is modelled using elastic beam/column elements fully restrained at the base section of the two columns, neglecting the foundation beam. The choice to neglect the nonlinear behaviour of the frame is justified by the slight or inexistent damage observed in the out-of-plane tests.

For each model, representative of one masonry typology, the structural response is obtained performing non-linear incremental static analyses (pushover), where two distinct loading stages are considered: (a) self-weight loads and additional vertical forces of 200 kN, applied on the top of each column; (b) uniform pressure distribution applied orthogonally to the masonry infill wall with monotonic increasing intensity. The gravity/vertical loads are applied with the infill present in order to transfer the compression stress to the masonry.

The analyses are performed by the structural software HISRA, HIstorical STRuctural Analyses), where the 3D macro model have been implemented (Histra, 2015). An iterative Newton-Raphson method with arch-length algorithm is employed in order to highlight the softening behaviour of the materials.

5.1 Estimation of key material mechanical properties

The flexural stiffness (*EI*) of the frame columns and beams are obtained considering a homogenized cross section and a secant Young modulus (*E*) of the concrete equal to 16.500 MPa, being representative of a cracked section.

The masonry compression strength is estimated from compression tests performed on masonry wallets within the research framework described in section 2. The flexural and sliding mechanical parameters of masonry, necessary to calibrate the non-linear links of the macro-model, are estimated from the out-of-plane bending tests performed on *system 1* and *system 2*.

5.1.1 Flexural parameters

In order to characterize the flexural behavior of masonry along the parallel and perpendicular directions to the bed joints, three out-of-plane bending specimens were tested in each direction according to (EN1052-2, 1999) for both types of brick masonry. The masonry specimens were laid on general purpose mortar and for the head joints both systems present interlocking joints. In the case of *System1*, the masonry specimens had 1300x765mm^2 and 1000x750mm^2 for the parallel and perpendicular direction to the bed joints respectively, see Figure 11 a,b. In the case of *System2*, the masonry specimens had 1000x600mm^2 and 1200x800mm^2 for the parallel and perpendicular direction to the bed joints, see Figure 11 c,d. Four lvdt's were used to control the displacement of the specimen, two under the loading sections (lvdt1 and 3) and two on the middle span (lvdt 2 and lvdt4) of the specimen (one on each side), see Figure 11. The force is measured using a loading cell attached at the end of the hydraulic actuator.

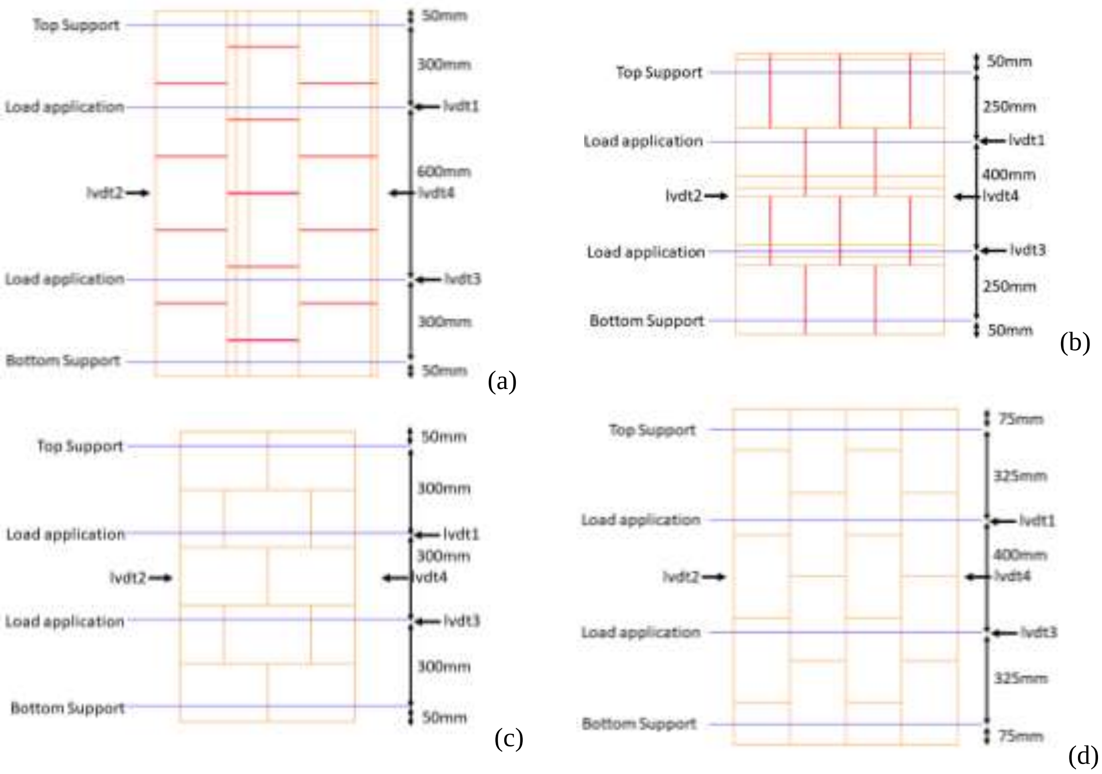

Figure 11 Specimens used for flexural tests; (a) System1 – parallel direction to the bed joints; (b) System1 – perpendicular direction to the bed joints; (c) System2 – parallel direction to the bed joints; (d) System2 – perpendicular direction to the bed joints.

The masonry Young modulus, parallel ($E_{//}$) and perpendicular ($E_{\perp}$) to the bed joints, is estimated by fitting the initial stiffness obtained from the experimental force-displacement diagrams whereas the masonry tangential modulus (G) is assumed 40% of the Young modulus. According to (Lourenco, 1997), the tensile strength of masonry (f_t) along the main directions of the material is estimated from the ultimate bending moment (M_u) obtained through the corresponding flexural test, using the expression:

$$f_t = M_u / 2W = F_u \, b / 4W \quad (1)$$

where F_u is the ultimate external load recorded during the test (average value from all specimens), b is the distance between the application point of external force F and the supports (see Figure 11) and W is the cross-section modulus. The tensile fracture energy g_t, associated to the experiment, is given by Eq. (2) where u represents the current deflection of the loaded point corresponding to the external force F and A_t the cross section of the specimen. The results are summarized in Table 1. The symbol (//) and ($\perp$) are used to indicate the test parallel and perpendicular to the bed joints respectively.

$$g_t = \frac{1}{A_t} \int F(u)du \tag{2}$$

Table 1 - Determination of the masonry tensile strength and fracture energy.

Typology	test	F_u [kN]	G_t [kNmm]	M_u [kNmm]	$A \cdot 10^3$ [mm^2]	$W \cdot 10^4$ [mm^3]	f_t [Mpa]	g_t [N/mm]
System1	//	2,64	37,56	396	76,5	127	0,14	0,501
	$\perp$	1,55	35,29	193	75,0	125	0,07	0,460
System2	//	2,49	3,84	373	84,0	196	0,08	0,046
	$\perp$	6,52	15,26	1059	112,0	261	0,16	0,135

Figure 12 and Figure 13 show the experimental and numerical flexural force-deflection curves, both in the parallel and perpendicular direction to the bed joints. The numerical results were obtained for different values of fracture energy. Hence, the results highlight the high influence of the fracture energy in the numerical response, mainly in the post-peak branches. On the contrary, little influence is observed until the peak-load is attained.

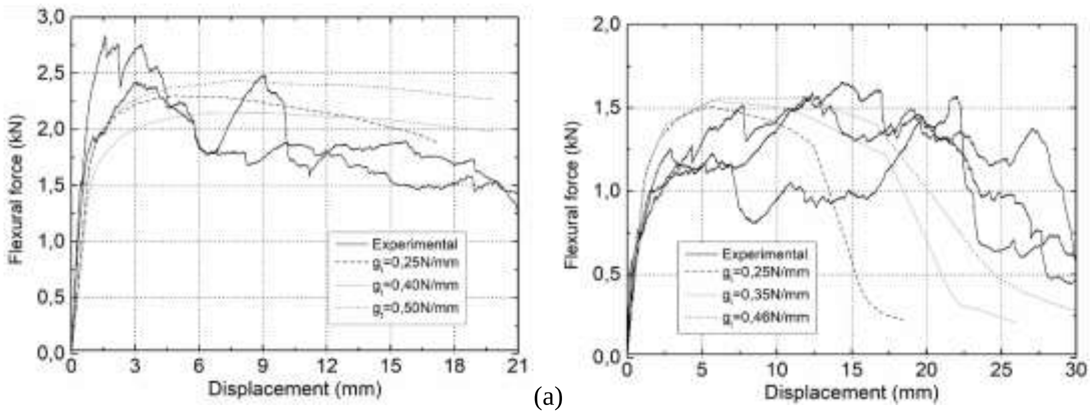

(a) (b)

Figure 12 Numerical simulation of the bending tests carried out in *System*1; (a) direction parallel to bed joints; (b) direction perpendicular to bed joints

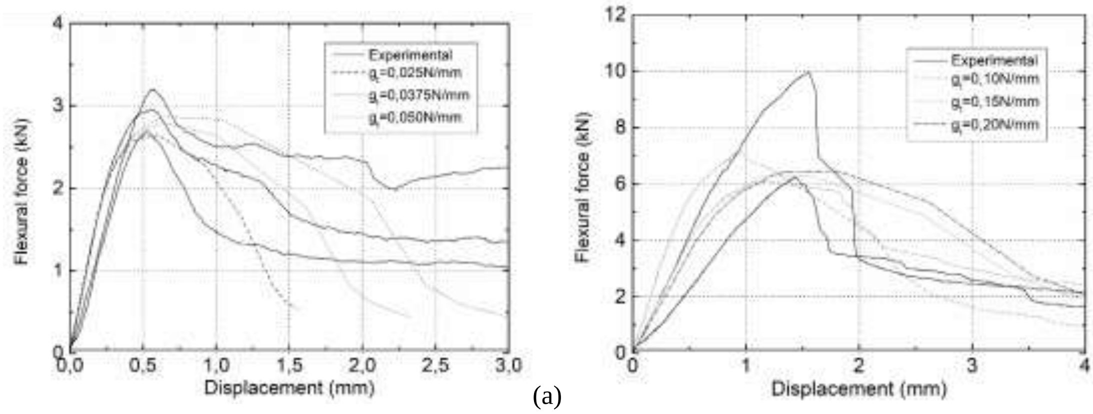

(a) (b)

Figure 13 Numerical simulation of the bending tests carried out in System2; (a) direction parallel to bed joints; (b) direction perpendicular to bed joints

5.1.2 The sliding properties

The mechanical parameters characterizing the sliding behaviour of the masonry bed joints are estimated through the numerical simulation of the flexural tests parallel to the bed joints (Figure 11a,c) by means of a meso-scale modelling approach, here performed employing the *DMM* described in section 4, as described in section 5.4. The flexural behaviour of the interfaces is calibrated according to the results obtained in the previous section, while their sliding behaviour is characterised assuming a constant friction coefficient μ=0,57, representative of the residual friction factor. The cohesion (c) and sliding fracture energy (g_{sl}) of the mortar joints are estimated fitting the experimental results of each system. Subsequently, parametric analyses are performed in order to estimate the influence of these parameters on the global response. The results of the parametric analyses, with reference to *system-2,* are shown in Figure 14. More in detail, the influence of the fracture energy is assessed by keeping the cohesion constant (*0,15MPa*) and varying the sliding energy (*0,025-0,050N/mm*) (Figure 14a). The influence of the cohesion is analysed by keeping the fracture energy constant (*0,025N/mm)* and by varying the values of cohesion (*0,15MPa and 0,23MPa*) (Figure 14b). The set parameters which led to the best approximation of the experimental results were $c=0,40MPa$ and $g_{sl}=0,1N/mm$ for *System1* and $c=0,15MPa$ and $g_{sl}=0,025N/mm$ for *System2*.

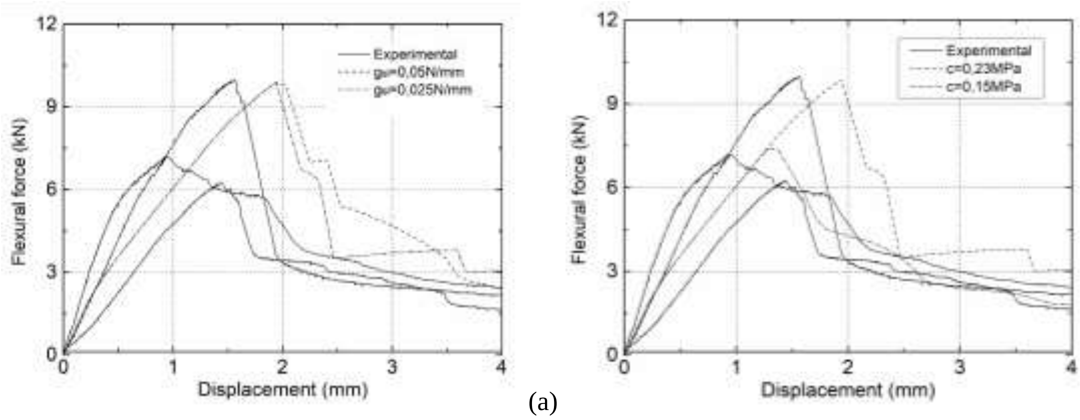

(a) (b)

Figure 14 Influence of the sliding fracture energy (a) and cohesion (b) on the out-of-plane flexural behaviour of the system-2 brick masonry.

The masonry compressive strengths (f_c) and the fracture energy in compression (g_c) are assessed using the results of compression tests performed on masonry wallets within the same research framework. In the numerical analyses, the same value of g_c=0,5N/mm is assumed for both masonry typologies. The other mechanical masonry parameters, adopted in the numerical simulations of the infill frame prototypes, are reported in Table for System1 and in Table for System2.

Table 2 - Mechanical property of the System-1.

Direc.	E [N/mm^2]	G [N/mm^2]	f_c [N/mm^2]	f_t [N/mm^2]	g_c [N/mm]	g_t [N/mm]	c [N/mm]	μ [-]	g_{sl} [N/mm]
Parallel	1200	450	3,00	0,14	0,5	0,50	0,4	0,57	0,10
Perpen.	250		1,00	0,07		0,46			

Table 3 - Mechanical property of the System-2.

Direc.	E [N/mm^2]	G [N/mm^2]	f_c [N/mm^2]	f_t [N/mm^2]	g_c [N/mm]	g_t [N/mm]	c [N/mm]	μ [-]	g_{sl} [N/mm]
Parallel	750	300	1,50	0,08	0,5	0,04	0,15	0,57	0,025
Perpen.	750		1,50	0,16		0,14			

5.2 Numerical simulation of the out-of-plane behaviour of the System 1(unreinforced)

The performance of the macro-modelling approach applied in the numerical simulation of the rc frame with masonry infill S*ystem1* (unreinforced*)* is compared with the experimental force-displacement diagrams (monotonic capacity curves) and damage patterns, see Figure 15 and Figure 16.

From the comparison of the numerical and experimental capacity curves, it is seen that the response of the models is close to the experimental curve, both in terms of lateral stiffness and ultimate strength. In particular, the numerical curve follows the experimental envelope in the pre-peak stage and in the first part of the post-peak branch with a very reasonable approximation. However, at 30mm of lateral displacement the numerical analysis is prematurely interrupted due to numerical convergence problems.

Figure 16a presents the mesh deformation of the macro-model at the last step of the analysis, while Figure 16b shows the corresponding damage scenario in terms of normal plastic deformation and sliding mechanisms. The first are represented by a grey colormap scale, defined according to (Pantò et al. ,2017), while the sliding is indicated by red lines.

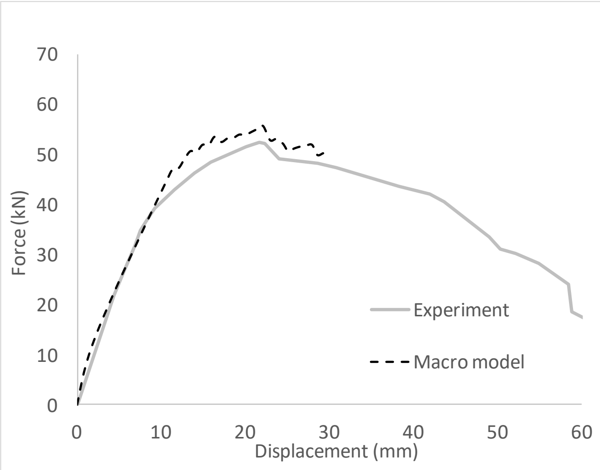

Figure 15 Comparison of the numerical and experimental capacity curves of the unreinforced prototype.

The numerical failure mechanism highlighted in Figures 15 is substantially coherent to the experimental observations briefly summarised in section 2. The tensile cracking is concentrated in the central part of the infill, where the highest bending moments are reached. A spread damage, characterised by plastic sliding, is observed along the diagonal directions of the infill and at the frame corner areas.

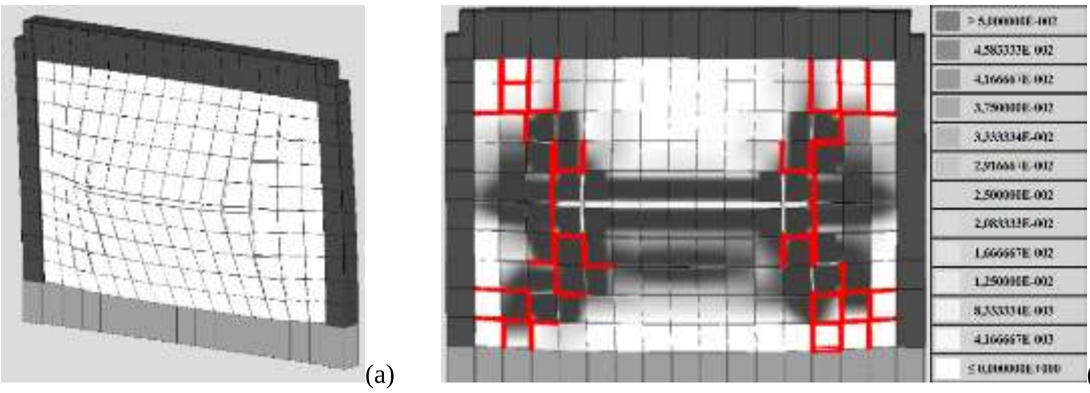

(a) (b)

Figure 16 Macro-modelling of the rc frame with *System 1* (unreinforced): (a) deformed mesh and (b) plastic damage at the last step of the analysis.

5.3 Numerical simulation of the out-of-plane behavior of the System 2 (unreinforced)

The experimental behaviour of masonry infill *System2* was characterised by sliding between the infill and the top beam of the frame. In the numerical analyses this aspect is well simulated when the infill-beam cohesion (c_{m-f}) is assumed to be equal to 65% of the masonry cohesion ($c=0.15MPa$). Figure 17 presents the numerical capacity curve obtained by means of the macro-model, together with the experimental envelope. It is considered that the model satisfactorily reproduces the experimental response until the lateral drift of 25mm although a slight underestimation of the initial lateral stiffness is observed. On the contrary, a good prediction of the ultimate strength of the system is provided.

In the post-peak stage, the numerical macro-model shows a sharper strength degradation, underestimating the actual ductility which the system exhibited during the experiment. This difference may be caused by the inability of the model to reproduce the large masonry deformations characterising the post-peak infill response since the hypothesis of small displacements and small deformations are accepted in the numerical simulations.

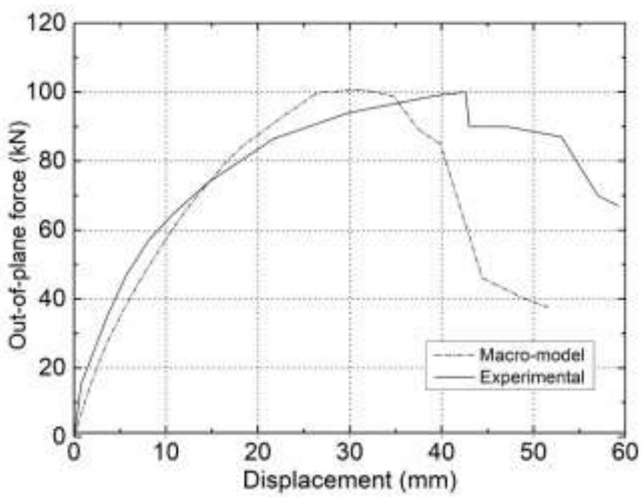

Figure 17 Comparison of the numerical and experimental capacity curve of the Unreinforced Infill Frame.

The plastic damage corresponding to the peak-load state is composed by tensile cracks concentred at the centre of the infill (Figure 18a) and at the base (Figure 18b). Widespread sliding develops in the horizontal and vertical interfaces along the diagonals of the infill. The last step of the analysis is characterized by widespread tensile cracking formed at the centre of the front face panel, at approximately 1/3 of the height from the base, and two vertical cracks, located at the 1/3 of the infill span from the columns (Figure 19a). Tensile cracks are concentred at the base section of the back face of the specimen (Figure 19b). The numerical collapse mechanism, described above, is substantially coherent with the experimental observations, both in terms of shape lateral deformation and plastic damage distribution.

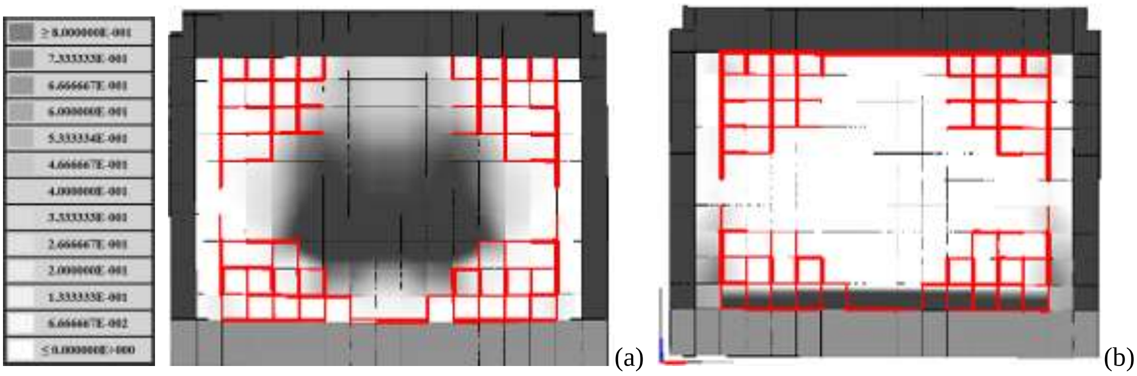

Figure 18 Damage distribution of the unreinforced infill frame at the peak load value: (a) front face ; (b) back face

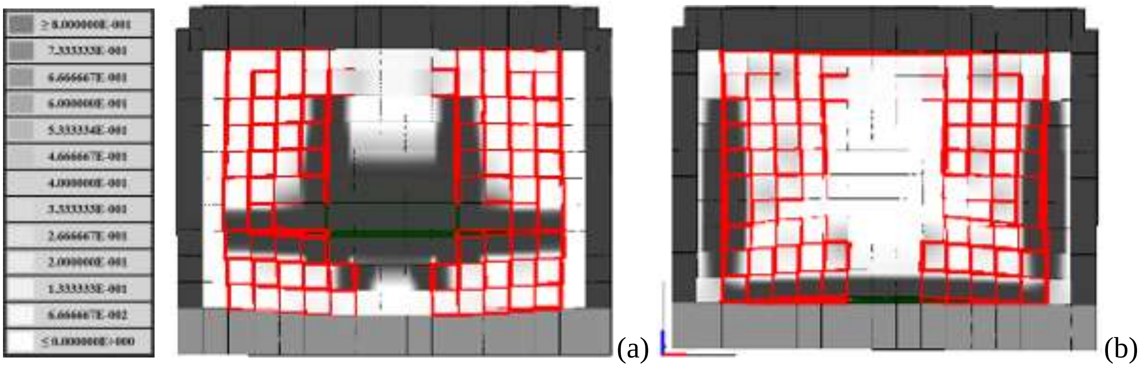

Figure 19 Damage distribution of the unreinforced infill frame at the last step: (a) front face ; (b) back face

5.4 Meso-scale numerical simulations

In order to validate the performance of the macro-model, two meso-scale models are developed. In these models, the actual masonry texture of each system is reproduced as shown in Figure 20b and 20c. According to this modelling strategy (Dolatshahi and Aref, 2011) (Macorini and Izzuddin, 2011) the masonry units are modelled using continuum solid or rigid elements, whereas the mortar layers are modelled by means of non-linear zero-thickness interface elements.

In the present study, the meso-scale models are developed employing the same macro-element described in section 4, calibrated in order to transfer the shear and normal masonry deformation to the diagonal and interface links. Each discrete element is defined to represent a single brick and is assigned to represent both the brick and the surrounding mortar joint properties according to the correspondence reported in Figure 20a. The interface nonlinear links are delegated to represent the mortar joints and the deformability of bricks according to the influence area of each link (Caliò and Pantò, 2014).

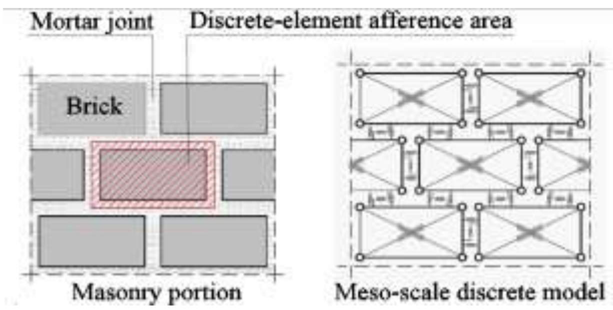

(a)

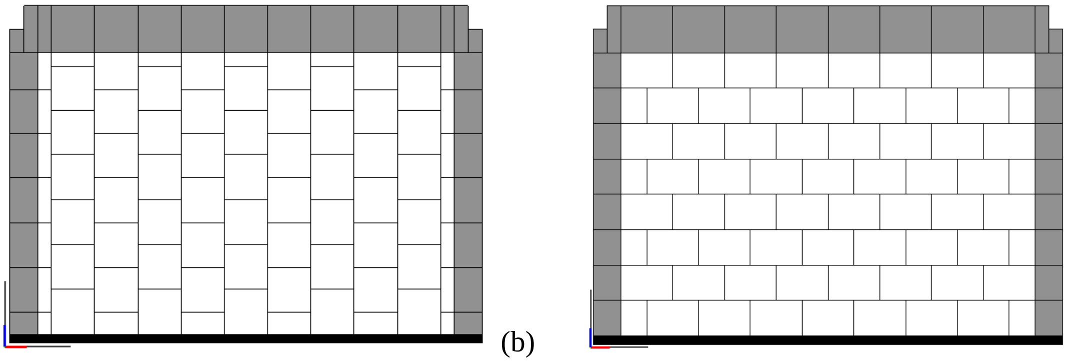
(b) (c)

Figure 20 Meso-scale modelling approach: mechanical scheme of the discrete model (a); discretization mesh of System-1 (b) and System-2(c).

Figure 21 shows the failure mechanism (last step of the analysis) obtained by means of the meso-scale model for the *system-1* with the distribution of the plastic damage on the interfaces. Similarly to the macro-model, the plastic deformations normal to the joints are represented by a gray colour map, while the sliding is represented by red lines. The numerical failure mechanism is characterised by tensile cracking at the central part of the infill and sliding at the beam/column joint areas. Due to the particular disposition of the bricks, the sliding mechanisms appear mainly along the vertical interfaces with a typical "*zig-zag*" shape, frequently observed in the brick masonry typologies.

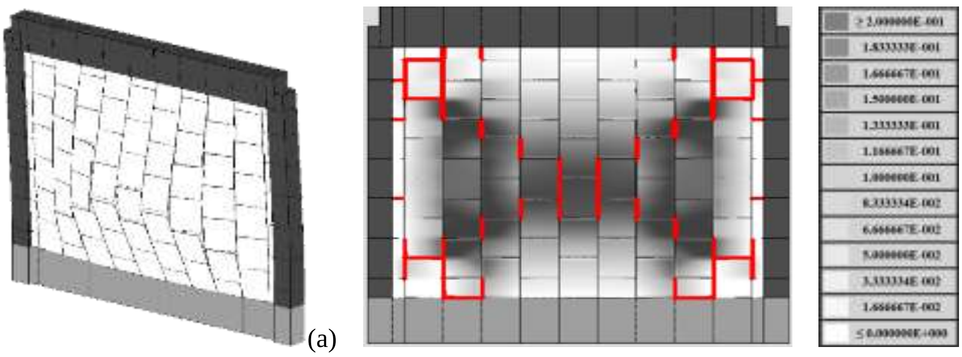

(a) (b)

Figure 21 Meso-scale model of the rc frame with *System 1* (unreinforced): (a) deformed mesh (b) collapse mechanism

It is interesting to notice that in this case, the horizontal cracks are more close to the base of the walls, similarly to the crack pattern visible in the specimens tested experimentally. This appears to indicate that in this constructive solution, the meso-scale modelling strategy can be more appropriate for the simulation.

The failure mechanisms of *system-2* predicted by the meso-scale discretization, considering three different values of infill-frame cohesion c_{mf} = 35% (model 1), 65% (model 2) and 100% (model 3) of the cohesion considered for the masonry joints, are reported in Figure 22. A significant influence of this parameter on the plastic damage distribution is observed: in *model 1*, the damage is more concentrated at the panel base and 3/4 of the panel height with two main horizontal tensile cracks and sliding along the horizontal mortar joints. Decreasing the cohesion (*model 2*, *model 3*), the plastic damage moves towards the top part of the infill wall.

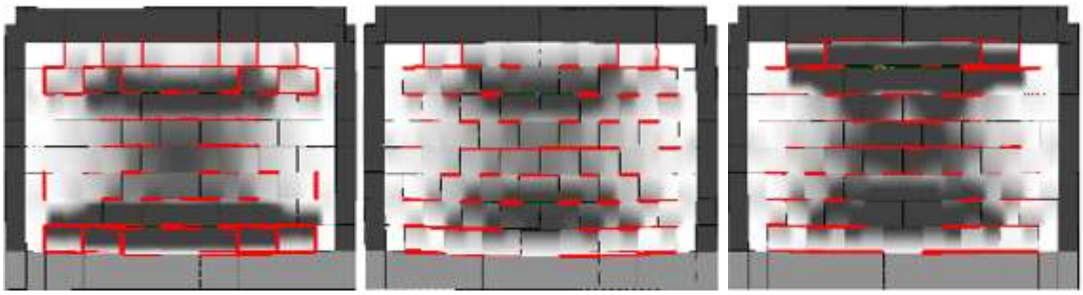

Figure 22 Plastic damage at the last step of the analysis for the model 1 (a), model 2 (b) and model 3 (c).

The comparisons between the numerical capacity curves are reported in Figure 23, where the experimental curves are also reported. A substantial agreement between the two models can be observed, mainly for the *system-1* where the two numerical curves are very close to each other. With regards to the *system-2*, a slight overestimation of the lateral strength is observed by the meso-scale model 3 ($c_{mf} = c$) if compared with the macro-modelling and the specimen. However, all three meso-scale models are rather close to the experimental curve providing a more reliable prediction of the initial lateral stiffness of the system, in comparison to the macro-model. However, the analyses performed on the meso-scale models are precociously concluded, approximately at 30mm, for problems concerning numerical stability of the solution.

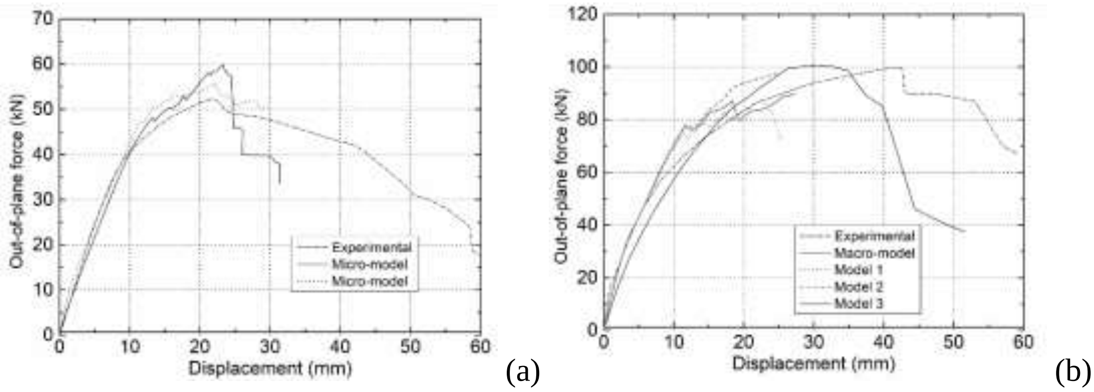

Figure 23 Capacity curves of the meso-scale models of the System-1 (a) and System-2 (b).

In conclusion, the comparisons reported in this sub-section confirmed that the macro-model is able to simulate the out-of-plane behaviour of brick infill frame systems with an accuracy comparable to the one obtained employing more refined meso-scale moelling strategies.

6 Simulation of the out-of-plane behaviour of the reinforced prototypes

As already described in section 2, two different reinforcing techniques have been considered and experimentally tested for the two brick masonry infill solutions. The reinforcement of *system-1* is constituted by vertical steel bars applied on the two external faces of the bricks through cementitious mortar to guarantee the tangential adherence between the bars and bricks. *System2* has been reinforced by means of horizontal steel bars located inside the mortar bed joints and mechanical connections between the infill and the columns.

Two different modelling approaches are used to simulate the behaviour of the two reinforced systems. In the case of *System1*, the reinforcing steel bars are explicitly modelled by means of additional macro-elements interacting to the other elements of the model by means of non-linear interfaces able to simulate the normal and tangential bond interaction between the reinforcing bars and masonry. For *System2*, since the reinforcement is embedded within the bed mortar joints, it is not possible to explicitly consider it by the macro-modelling strategy. For this reason, the reinforced infill is modelled as an equivalent homogenised material with increased flexural mechanical properties related to the ones adopted to model the unreinforced infill.

6.1 The System1 prototype

The reinforcement is modelled following the approach proposed by (Caddemi et al., 2017), in which the reinforcing steel bars are simulated by means of piecewise rigid plates interacting to the masonry by means of zero thickness non-linear discrete interfaces. The latter simulate the cohesive behaviour of the mortar layer connecting the bars to the masonry, in normal and tangential directions. Each interface is made of a row of *n* transversal N-Links which simulate the normal interaction (k_n) and of a single longitudinal N-Link which simulates the shear behaviour (k_s). Figure 24 presents a simplified modelling scheme of a portion of the reinforced masonry infill through an assemblage of macro-elements and rigid plates corresponding to the reinforcement system.

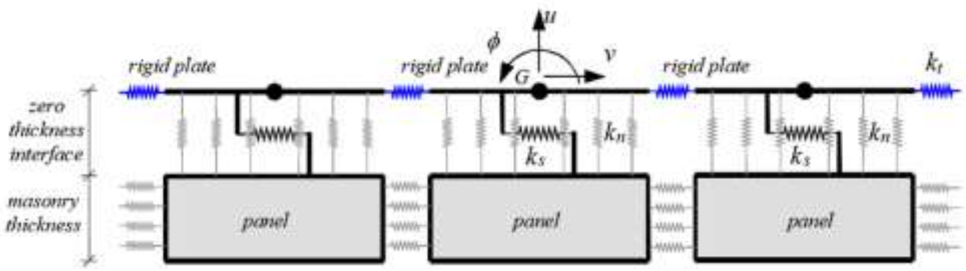

Figure 24 Modelling scheme of the reinforced system.

Each plate is characterized by three degrees of freedom, associated to the two translations of its barycentre (u,v) and to the rotation of the plate (ϕ). According to the philosophy of the macro-modelling approach, the rigid plates are discretized by a mesh compatible to the mesh of the macro-elements (Figure 24). The plates interact with each other by means of unidirectional links (k_t) working only in traction which reproduce the deformability and strength of the bars under tension. This mechanical behaviour is described by an elastic-brittle constitutive law characterised by the elastic Young modulus (E_s) and yield stress (f_y) of the steel and the area of the bar (A_t).

An elasto-plastic bond-slip constitutive law with linear softening behaviour, characterised by the yield tangential stress (τ_s) and the ultimate fracture energy (g_s), is employed to simulate the debonding failure mechanism of the reinforcements. The geometrical and mechanical parameters of steel bars and the bond-slip constitutive parameters, necessary to mechanically calibrate the model, are estimated according to (Caddemi et al. ,2017) and reported in Table 4.

Table 4 - Mechanical parameters of the reinforcing steel bars and the bond-slip constitutive law

Tensile behaviour			Bond-slip behaviour		
E_s [MPa]	f_y [MPa]	A_t [mm^2]	k_s [N/mm^3]	τ_s [MPa]	g_s [N/mm]
210000	547.35	28	600	0,4	0,5

Figure 25 shows the plastic damage distribution at the last step of the pushover analysis. It can be observed that the plastic damage is constituted by masonry flexural cracking on the infill masonry and sliding between masonry and reinforcements. The latter, mostly concentrated at the bottom part of the front face panel (Figure 25a), is indicated by red lines, similarly to the representation adopted for the sliding mechanisms between two masonry panels. At the back face, tensile cracking occurs at the base section of the infill and near the columns, while sliding is activated in correspondence of the interfaces between the infill and the columns (Figure 25b).

This failure mode is rather different from the collapse mechanism exhibited by the unreinforced brick masonry infill. The widespread tensile cracking at the central part of the panel and sliding at the corners, observed in the unreinforced model, are here strongly restricted by the confinement action of the reinforcements.

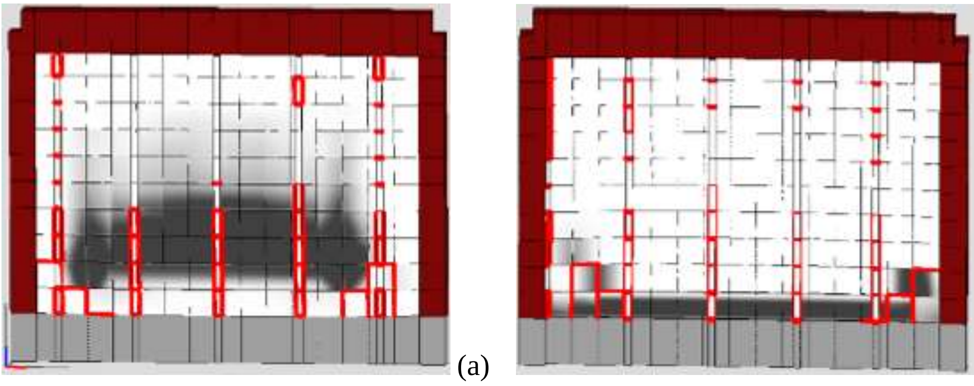
(a) (b)

Figure 25 Damage distribution at the last step of the analysis; front face (a), back face (b).

The numerical capacity curve is reported in Figure 26 compared to the experimental monotonic envelope. From this, it is possible to observe a good agreement between numerical and experimental response in terms of lateral stiffness, ultimate load and displacement capacity. Two phases can be recognized in the numerical response: (1) from zero to approximately 55kN, numerical and experimental response are very close; (2) after the out-of-plane resistance of 55kN, the numerical response is characterised by an irregular path with continuous loss of strength, due to the sliding mechanism involving the reinforcement. This leads to numerical values of out-of-plane resistance slightly lower than the ones recorded in the experimental test.

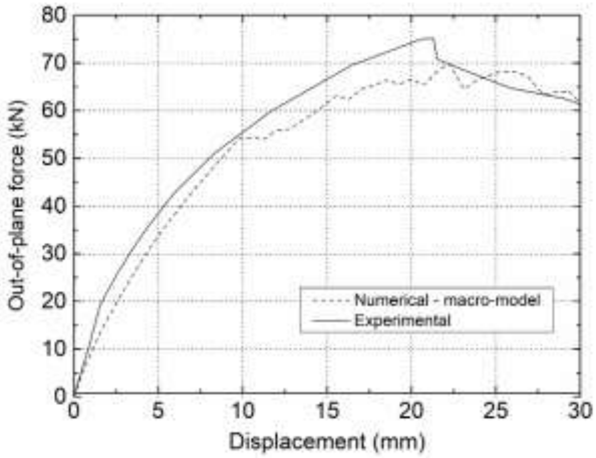

Figure 26 Numerical and experimental capacity curve of the reinforced prototype.

A more refined mesh of the reinforcing steel bars would be necessary to more accurately follow the progressive loss of reinforcement adherence. Nevertheless, the adopted mesh discretization gives a satisfactory prediction of the global strength of the reinforced system, coherently to the simplified character of the modelling approach.
The difference between the experimental strength and the numerical prediction is approximately 10%. This level of approximation is considered to be adequate to the scope of the numerical investigation.

6.2 The System2 prototype

The contribution of the steel reinforcements, applied within the horizontal bed joints, is modelled increasing the masonry tensile strength and fracture energy, along the direction parallel to the bed joints. Furthermore, in order to take into account, the steel connections between infill and frame, the sliding motion at the masonry-column interfaces is inhibited. The new flexural parameters of the masonry are estimated by simulating the flexural tests performed on reinforced specimens and fitting the experimental results. The tensile strength (f_t) of the reinforced masonry was evaluated yet again as $M_u /2W$ resulting in the value of 0,83 MPa, being the ultimate moment M_u equal to 4371 KNmm. The corresponding tensile fracture energy (g_t) that adequately provides the experimental results is 4,00 N/mm. Figure 27 shows the influence of the fracture energy on the force-deflection bending test response. It is important to notice that the reinforcing system produces an extreme increase of the masonry ductility when compared to the unreinforced masonry system.

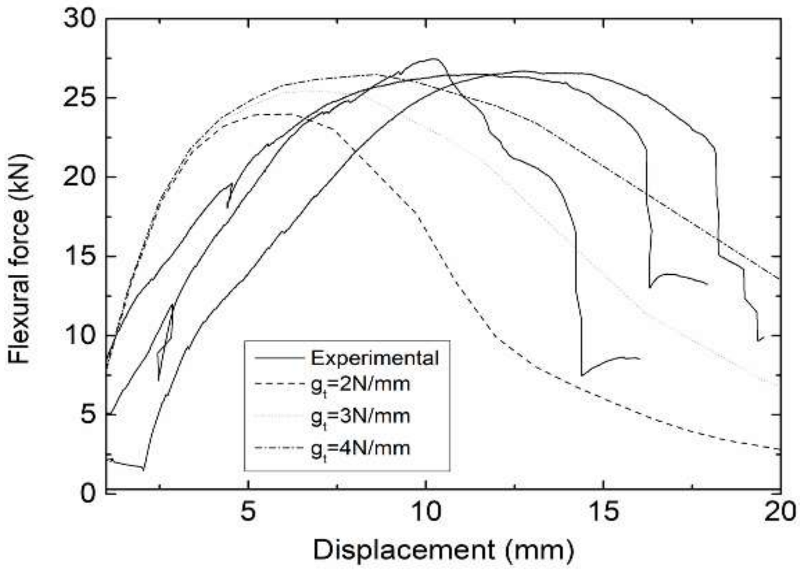

Figure 27 Numerical simulation of the bending tests on the reinforced masonry walls : influence of the tensile fracture energy

Figure 28 shows the failure mechanism and the corresponding plastic damage distribution of the reinforced system. The numerical damage scenario is substantially coherent to the results of the experiments. In order to better clarify the difference between the unreinforced and reinforced system, the ultimate lateral displacements obtained with and without reinforcements are compared, see Figure 29. The two scenario are sensibly different: in the unreinforced masonry infill (Figure 29a) the peak lateral displacement is recorded below the central section of the panel; in the reinforced prototype (Figure 29b) the peak lateral drift is achieved at the top of the infill. It is seen that in both cases the detachment of the walls from the top beam occurs but the failure of the reinforced model is more influenced by sliding between the infill and the top rc beam.

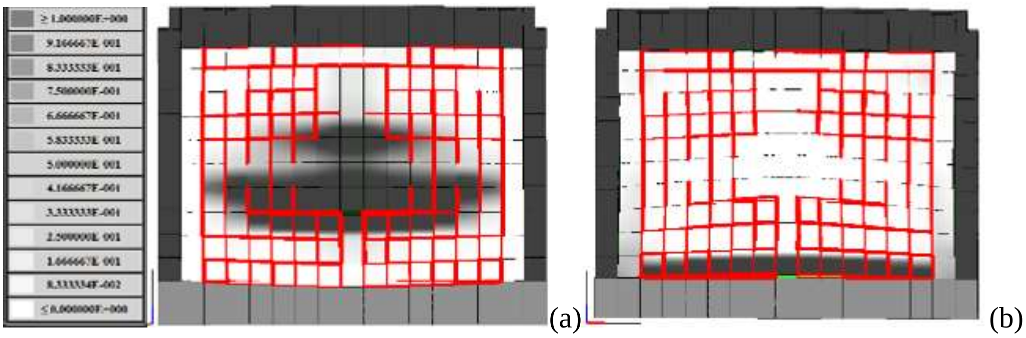

Figure 28 Damage distribution of the unreinforced infill frame at the last step: (a) front face (b) and back face.

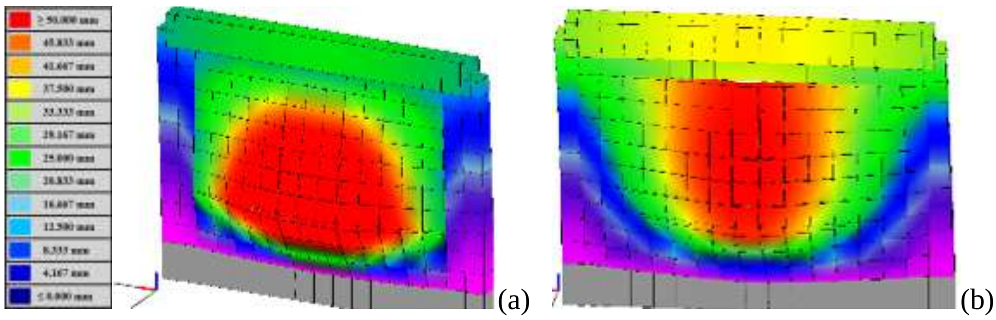

Figure 29 Comparison of the ultimate deformed shape of: (a) unreinforced masonry infill wall ; (b) and reinforced masonry infill wall.

The considerable increment of the tensile strength and ductility of masonry along the horizontal direction due to the reinforcing system, lead to predominant horizontal bending. This enabled the infill to carry increment of lateral load although large horizontal cracks are developed by means an horizontal bending moment transfer mechanism.

The comparison between numerical and experimental capacity curve, is reported in Figure 30, from which it is possible to see that a substantial agreement between the responses, both in terms of initial lateral stiffness and ultimate load-carrying capacity.

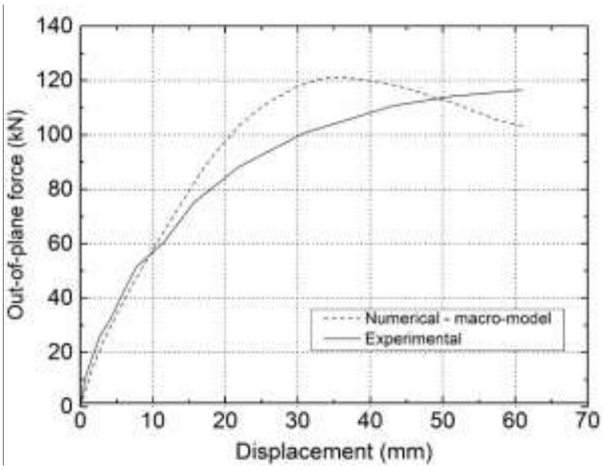

Figure 30 Numerical capacity curve compared to the experimental results.

Up to the lateral displacement of 15 mm, the numerical and experimental curves are very close to each other. After this point, the numerical model begins to overestimate the lateral stiffness of the system, reaching the peak load before the specimen, at a lateral drift of approximately 35mm. The model then shows a softening branch, which leads the numerical prediction towards the experimental curve. The discrepancies between the numerical and experimental curve can be justified by the simplicity of constitutive law employed to simulate the out-of-plane sliding mechanism. A non-linear plastic constitutive law, instead of the elasto-plastic here considered to calibrate the longitudinal interface links, may give a better approximation of the experimental response. Nevertheless, it is considered that the current modelling accuracy level is satisfactory to interpret the global structural behaviour of the system and suitable to be used in real structures for seismic vulnerability assessments.

7 Parametric analyses

In order to assess the sensitivity of brick masonry infill walls on the main mechanical and geometrical parameters and evaluate how they influence the lateral stiffness and strength of the system, it was decided to perform a parametric study. This study refers to *System2 which can be considered representative of traditional masonry infills*. Five aspects are considered, as shown in Table 5: infill geometry including thickness (t) and infill aspect ratio (L/H); masonry strength including compression strength (f_c), tensile strength (f_t), tensile fracture energy (g_t), cohesion (c), friction coefficient (μ) and sliding fracture energy (g_s); masonry stiffness (E_m, G_m); opening effects; vertical loads, applied in the columns (Q) and in the top rc beam (q). Regular opening distribution, constituted by a single central door or window opening, characterized by different geometrical ratio A_O/A_m, where A_O is the area of opening and A_m the area of the masonry infill wall, is here considered.

A set of three values is taken into account for each parameter investigated namely, an average value (v_m) and two upper/lower values (v_{inf} / v_{sup}) obtained by an increase or a decrease of 50% to 100% of the average value, v_m. The numerical analyses were performed considering the variability of a singular parameter, whereas the others were kept constant and equal to the average values as reported in Table 5.

Table 5 - Geometrical parameters considered in the sensitivity analysis (N-mm).

Aspect investigated	parameter	symbol	measure unit	values		
				v_{inf}	v_m	v_{sup}
Infill geometry	thickness	T	-	100	140	210
	In-plane shape ratio	L/H	-	1,00	1,50	2,00
Masonry strength	compression strength	f_c	MPa	1,20	1,80	2,40
	tensile strength (isotropic behaviour)	f_t	MPa	0,10	0,25	0,50
	tensile fracture energy (isotropic behaviour)	g_t	N/mm	0,03	0,30	0,90
	cohesion	c	MPa	0,10	0,15	0,20
	friction factor	μ	-	0,4	0,55	0,70
	sliding fractural energy	g_s	N/mm	0,025	0,05	0,10
Masonry stiffness	Young modulus	E_m	MPa	600	1200	2400
	shear modulus	G_m	MPa	150	300	600
Openings	windows opening ratio	A_O/A_m	%	0	13	28

	door opening ratio	A_O/A_m	%	0	23	37
Vertical loads	column loads	Q	kN	50	200	300
	beam loads	q	kN/m	25	50	100

The results of the parametric analyses on the full infilled frames are reported in Figure 31 in terms of capacity curves expressed as base shear *vs* maximum lateral displacement. The strength parameters characterizing the sliding behaviour and, in particular, the sliding fracture energy (g_s), cohesion (c) and the friction factor (μ), influence the ultimate lateral strength of the system, see Figure 31g, h, i. The increase on the infill compression strength results in a slight increase of the peak system strength and ductility capacity (Figure 31e).

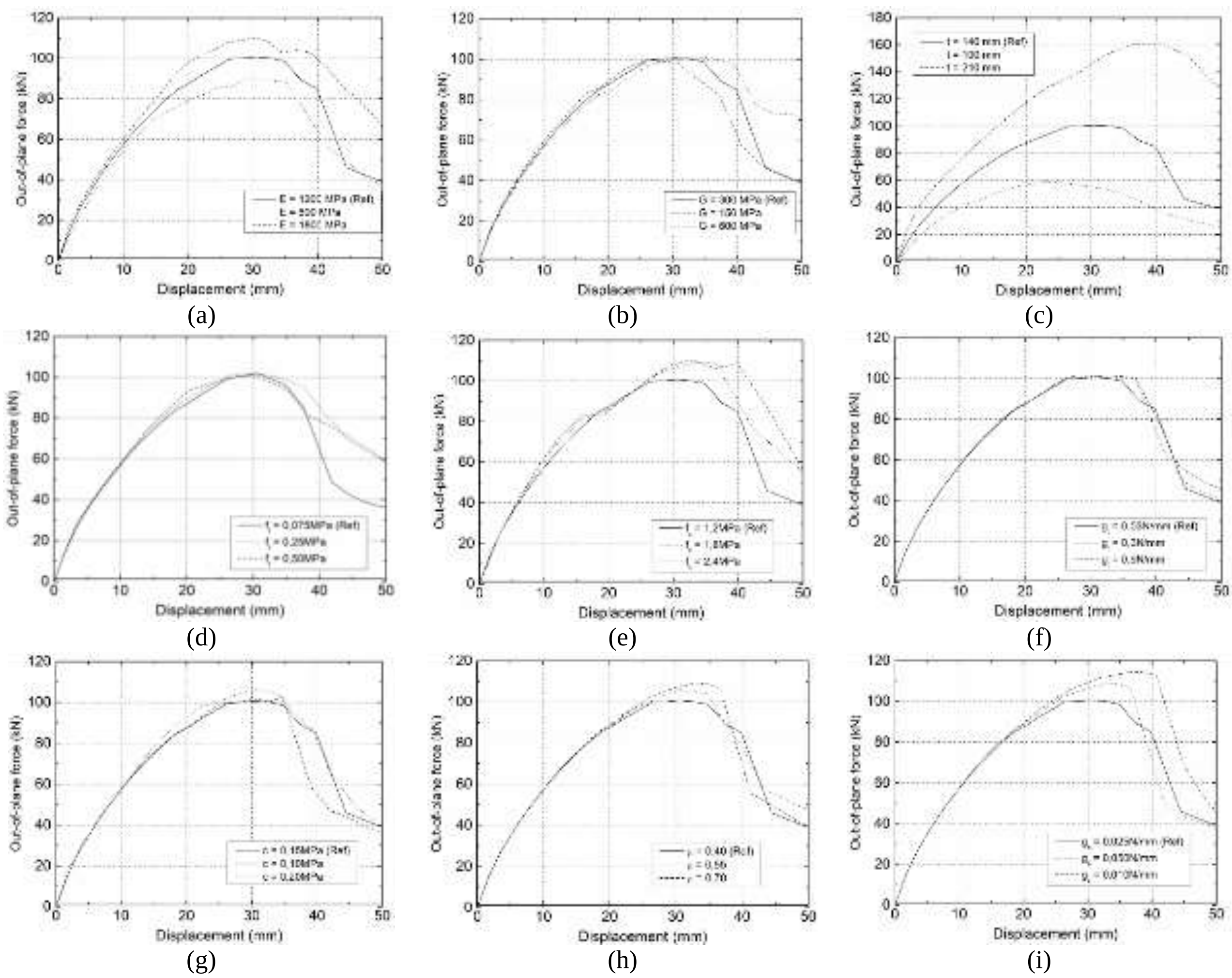

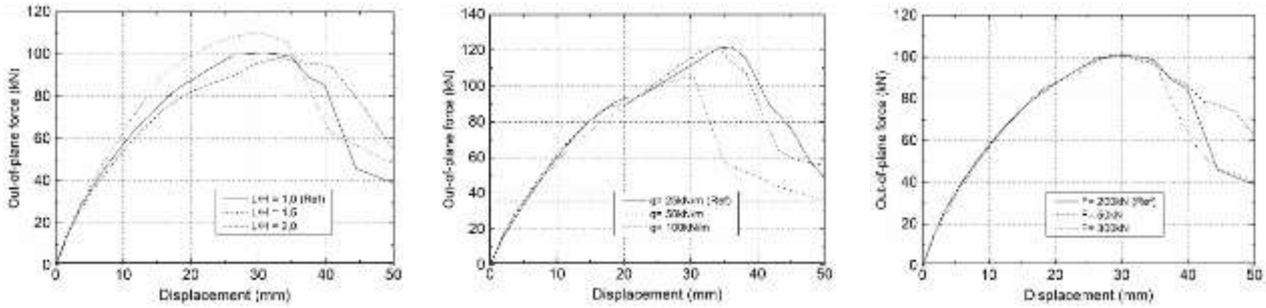

(m) (n) (p)

Figure 31 Sensitivity analysis of the macro-model: Young modulus (a); tangential modulus (b); thickness of infill (c); compression strength (d); tensile strength (e); tensile fracture energy(f); cohesion (g); friction coefficient (h); fractural sliding energy (i); infill shape ratio (m); vertical beam load (n); vertical loads on the column (p).

A low sensitivity of the model on the tensile fracture energy is observed (Figure 31f) while tensile strength influences only the post-peak response (Figure 31d). The initial stiffness is greatly influenced by the thickness of the infill (Figure 31c) and slightly influenced by the Young masonry modulus (*E*) as shown in Figure 31a. Conversely, shear modulus (*G)* influences only post-peak response of the system (Figure 31b). Finally, in-plane infill aspect ratio (*L/H)* considerably influences the peak and post-peak response, Figure 31m.

Distributed beam load (*q*) significantly influences the ultimate resistance of the system, see Figure 31n. High values of the distributed load results in a significant decrease on the out-of-plane resistance of the masonry wall. This is associated to the direct transfer of the vertical load to the brick infill, increasing the masonry compression stress state. Since flexural behaviour and arching mechanism prevail on the infill response, it is affected by the increase on the compression stress levels due to the development of anticipated crushing mechanism when out-of-plane load is applied. This brings to light the issue of deformability of the rc beams/slabs, inducing additional compressive stresses to the infill walls and reducing its out-of-plane resistance. On the other hand, it is observed that the vertical column forces (*F*) slightly influence the global response of the brick infill (Figure 31p), since such loads transferred directly by the stiffer r/c columns to the foundation.

The influence of the infill shape ratio was investigated keeping a constant height (*H*) while changing the system length (*L*). Typical damage patterns of brick infill, for two different aspect ratios are reported in Figure 32. The failure mode changes from the formation of two vertical and horizontal tensile cracks (case L/H=1) to the formation of a widespread horizontal crack in the case of L/H=2. In the first case a 2D-bending mechanism develops, whereas in the second case, a unidirectional (vertical) flexural mechanism predominates.

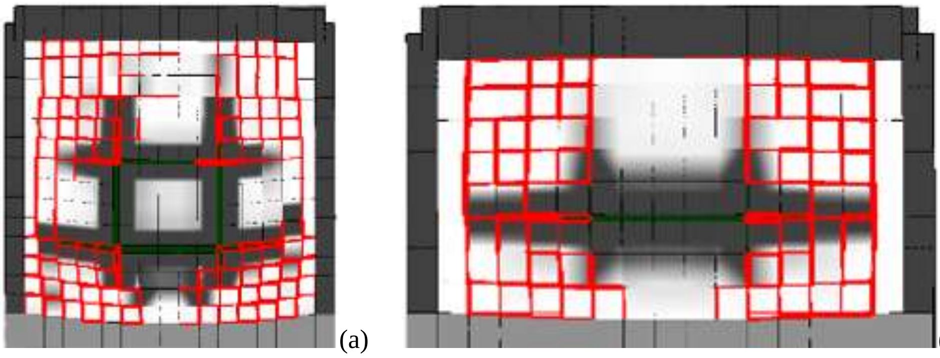

(a) (b)

Figure 32 Failure modes associated to the geometry ratio L/H=1(a) and L/H=2(b)

The responses of the masonry infills with different types of openings (windows and doors) and different percentages of opening area are shown in Figure 33. It is observed that the presence of openings produces a significant invariably reduction of the initial lateral stiffness of the system. A lateral strength reduction is observed in the door-open systems. On the contrary, window-opening results indicate no significant influence in the out-of-plane strength, despite the decrease of lateral stiffness.

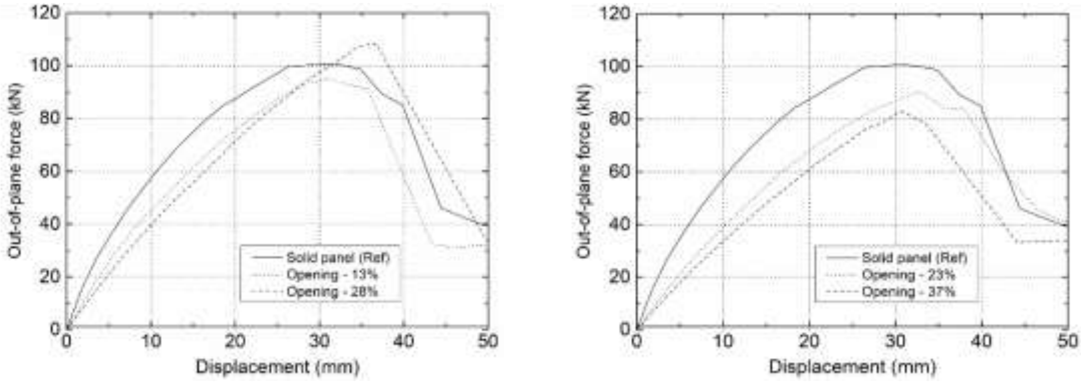

(a) (b)

Figure 33 Capacity curves of the infill frame with opening; (a) windows opening; (b) doors opening.

The collapse mechanisms observed for different openings are shown in Figure 34. The damage is concentrated mainly at the lateral sides of the openings. A more evident damage concentration is observed in the upper spandrel where infills are characterized by low opening ratio (windows 13% and door 23%).

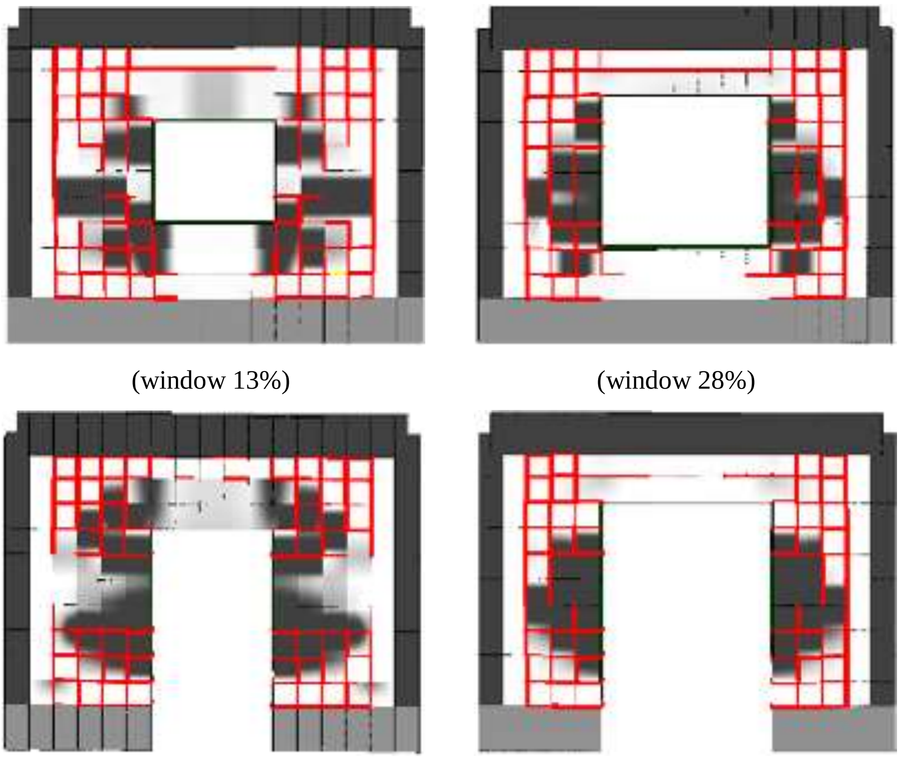

(window 13%) (window 28%)

(door 23%) (door 37%)

Figure 34 Collapse mechanisms of the infilled frame with opening.

7.1 Variation of the out-of-plane stiffness and strength

Taking into account the most influential parameters in the out-of-plane behavior of the investigated brick infill walls, it was decided to perform a deeper investigation on their influence in the variation of the ultimate strength (F_u) and initial stiffness (K_I), the latter evaluated at 30% of load level with respect to the peak.

Four dimensionless parameters are considered: (*i*) relative masonry-concrete deformation ratio (E_m/E_c) considering a constant concrete module E_C=30GPa; (*ii*) in-plane infill shape ratio (L/H); (*iii*) thickness ratio (t/H) and (*iv*) distributed vertical beam load (q) referred to the specific masonry self-weight ($q_m=Htw$). The values of the investigated parameters and the corresponding strength and stiffness are reported in Table 7.

Table 7 – Initial stiffness [kN/mm] and ultimate lateral load [kN].

Thickness ratio	t / H	0,04	0,05	0,06	0,07	0,08	0,09	0,10	0,12
	K_I	3.41	3.30	3.92	4.73	5.51	5.72	6.25	6.57
	Fu	23.94	35.47	49.04	63.79	78.83	95.62	113.97	140.98
In-plane aspect	L/H	1,0	1,2	1,4	1,6	1,8	2,0	2,5	
	K_I	7,07	6,40	6,23	6,49	5,91	6,21	5,43	
	Fu	110,36	104,26	100,15	100,64	96,00	98,37	93,23	
Masonry deformation	E_m / E_c	0,02	0,03	0,04	0,05	0,06	0,07	0,08	0,10
	K_I	5,35	5,55	5,76	5,90	6,00	6,08	6,15	6,21
	Fu	84,99	89,50	96,.87	100,71	104,52	106,74	108,91	110,20
Vertical load	q/q_m	0,05	0,15	0,3	0,5	0,65	0,05		
	K_I	6,09	6,20	6,38	6,63	6,82	6,34		
	Fu	118,59	121,92	121,94	123,21	117,32	104,89		

The out-of-plane resistance is clearly affected by the thickness ratio of the walls, being higher for increasing values of the thickness. The out-of-plane lateral stiffness also increases but at a lower rate. The masonry elastic modulus contributes to the increase of both stiffness and ultimate resistance however, at a lower rate than that associated to the increasing thickness ratio.

The vertical load applied in the rc beam has little influence on the out-of-plane strength for high load values. On the other hand, additional vertical loads make the system stiffer. The in-plane aspect ratio has an important influence in the out-of-plane resistance and lateral stiffness.

8 Conclusions

This paper presented the results of the numerical simulation of the mechanical behaviour of two modern solutions of brick masonry infill walls submitted to out-of-plane loading. The solutions of masonry infill walls intended to improve its behaviour under seismic loads. The numerical simulations are based on an innovative discrete-macro-modelling approach, able to simulate the in-plane and out-of-plane behaviour of infill frames with a reduced computational effort if compared to refined non-linear finite element approaches. Following this strategy, the frame is modelled by lumped plasticity beam/column elements whereas the infill is discretized by means of macro-elements consisting in articulated quadrilaterals connected to each other and to the frame through non-linear discrete interface elements, simulating both the axial/flexural and sliding, in-plane and out-of-plane, interactions.

In order to limit the sources of uncertainty, associated to the calibration of the model, the present study has been restricted on the simulation of the out-of-plane behaviour of undamaged systems. Thus, the influence of the in-plane motion and damage on the out-of-plane behaviour was neglected. Further investigations are needed to assess the in-plane out-of-plane interaction mechanisms and its numerical simulation.

Based on the results achieved, it is possible to drawn the following conclusions:

(a) it was possible to obtain the major mechanical properties to calibrate the numerical macro-element model developed for both infill masonry walls (unreinforced and reinforced) based on the results of the flexural tests;

(b) good agreement between experimental monotonic envelops and numerical pushover curves was attained, namely at the level of initial stiffness and out-of-plane resistance. After peak load is attained, the responses are more divergent which can be associated to the predominant arching mechanism observed in the experimental campaign and that cannot be described through the macro-element method.

(c) the crack and deformation patterns obtained in the numerical models were mostly compatible with the crack patterns and deformation paths obtained in the experimental out-of-plane tests.

(d) the parametric analysis revealed that geometrical features of the masonry infill walls play a central role on the out-of-plane behaviour of the brick infills, namely the length to height aspect ratio and the thickness to height ratio. Increasing values of the L/H ratio lead to the decrease on the out-of-plane resistance, which is justified by the changing on the governing resisting mechanism from two way bending to one way being. In addition, the out-of-plane stiffness decreases with increasing values of L/H. Besides, it is clear that low values of thickness to height ratio results (slenderness), result in very low values of out-of-plane resistance.

(e) the out-of-plane performance of brick infills is negatively affected by the uniformly distributed load on the top rc beam. In general, no additional vertical loads are supposed to be applied on the brick infills, given that they are considered to be non-structural. However, if for constructive imperfections or long-term behaviour additional loads are induced in the brick infills, these can contribute to increase its seismic vulnerability.

9 REFERENCES

Akhoundi, F., Vasconcelos, G., Lourenço, P., Silva, L. M., Cunha, F., & Fangueiro, R. In-plane behavior of cavity masonry infills and strengthening with textile reinforced mortar. Engineering Structures, 156 (December 2016), 2018, 145–160. https://doi.org/10.1016/j.engstruct.2017.11.002.

Akhoundi, F., Vasconcelos, G., Lourenço, P. B., & Silva, L., Out-of-plane response of masonry infilled RC frames: Effect of workmanship and opening. In 16th International Brick and Block Masonry Conference, 2016, Masonry in a world of challenges, 1147-1154. Taylor & Francis.

Angel R., Abrams D., Shapiro D., Uzarski J. and Webster M., Behavior of Reinforced Concrete Frames with Masonry Infills, Civil Engrg. Studies, Structural Research, Series No. 589, UILU-ENG-94-2005, 1994, Dept. of Civil Engineering, University of Illinois at Urbana Champaign.

Asteris P.G. (2008). Finite element micro-modeling of infilled frames. Electron J Struct.Eng. 2008; 8:1–11.

Asteris,P.G., Cavaleri, L., Di Trapani, F., Tsaris, A.K., Numerical modelling of out-of-plane response of infilled frames: State of the art and future challenges for the equivalent strut macromodels, Engineering Structures, 2017, 132, 110-122.

Braga F, Manfredi V, Masi A, Salvatori A, Vona M. Performance of non-structural elements in RC buildings during the L'Aquila, 2009 earthquake. Bulletin of Earthquake Caddemi S, Caliò I, Cannizzaro F, Lourenço PB, & Pantò B. FRP-reinforced masonry structures: Numerical modeling by means of a new discrete element approach.

Caddemi S, Caliò I, Cannizzaro F, Lourenço PB, Pantò B: FRP-reinforced masonry structures: numerical modeling by means of a new discrete element approach. 6th Int. Conf. on Comp. Meth. in Structural Dynamics and Earthquake Engineering, 2017, Rhodes Island, Greece. Engineering. 9, 2011, p. 307-324.

Caliò I, Marletta M, Pantò B. A new discrete element model for the evaluation of the seismic behaviour of unreinforced masonry buildings. Eng Struct 2012, 40, 327–38.

Caliò I, Pantò B. A macro-element modelling approach of Infilled Frame Structures. Computers and Structures, 2014, 143, 91–107.

D'Ayala D, Worthb J, Riddle O. Realistic shear capacity assessment of infill frames: comparison of two numerical procedures. Eng Struct 2009;31:1745–61.

Di Trapani F., Shing P. B., Cavaleri L. Macroelement Model for In-Plane and Out-of-Plane Responses of Masonry Infills in Frame Structures. Journal of Structural Engineering, 144(2), 2017, 04017198.

Dolatshahi K. M., Aref, A. J. Two-dimensional computational framework of meso-scale rigid and line interface elements for masonry structures. Engineering Structures, 33(12), 2011, 3657-3667.

Drysdale R, Essawy A. Out-of-Plane Bending of Concrete Block Walls. Journal of Structural Engineering 114, 1988, p. 121-133.

FEMA 461, Interim testing protocols for determining the seismic performance characteristics of structural and nonstructural components, 2007.

Flanagan R, Bennett R. Bidirectional Behavior of Structural Clay Tile Infilled Frames. Journal of Structural Engineering 125, 1999, p. 236-244.

Furtado, A., Rodrigues, H., Arêde, A., & Varum, H., Experimental evaluation of out-of-plane capacity of masonry infill walls, Engineering Structures, 2016, 111, 48-63.

Furtado A, Rodrigues H, Arêde A, Varum H. Simplified macro-model for infill masonry walls considering the out-of-plane behaviour. Earthquake Engineering & Structural Dynamics, 2016, 45: 507–524.

HiStrA (Historical Structure Analysis). HISTRA s.r.l, Catania, Italy. Release 17.2.3, April 2015.

Kent D. C., Park R. Flexural members with confined concrete. Journal of the Structural Division, 1971. (Proc. of the American Society of Civil Engineers), 1971; 97(ST7): 1969-1990

Insysme Project. Retrieved from http://www.insysme.eu/, 2017.

Lourenço PB. An anisotropic macro-model for masonry plates and shells: Implementation and validation. Delft University of Technology, Faculty of Civil Engineering 1997, Mechanics and Structures, Computational Mechanics.

Macorini, L., Izzuddin, B.A. (2011). ”A non-linear interface element for 3D mesoscale analysis of brick-masonry structures.” International Journal for Numerical Methods in Engineering. Vol:85, ISSN:0029-5981, Pages:1584-1608.

Madan A, Reinhorn AM, Mander JB, Valles RE. Modeling of masonry infill panels for structural analysis. J Struct Eng 1997;123(10):1295–302.

Marques R, Lourenço PB, Unreinforced and confined masonry buildings in seismic regions: validation of macro-element models and cost analysis. Eng.Struct. 2014, 64(52), 67.

Menegotto M., Pinto P.E. Method of analysis for cyclically loaded RC plane frames including changes in geometry and non-elastic behavior of elements under combined normal force and bending. Symp. Resistance and ultimate deformability of structures acted on by well defined repeated loads, IABSE 1973, Reports, 13, Lisboa.

McKenna F, OpenSees: a framework for earthquake engineering simulation. Computing in Science & Engineering, 13(4), 2011, p. 58-66.

NP EN 1998-1: Eurocódigo 8 - Projecto de Estruturas para resistência aos sismos. Parte 1: Regras gerais, acções sísmicas e regras para edifícios. Instituto Português da Qualidade, 2010.

Oliaee M, Magenes G. In-plane out-of-plane interaction in the seismic response of masonry infills in RC frames. In: Brick and block masonry: proceedings of the 16th international brick and block masonry conference, Padova, Italy; 26–30 June 2016

Pantò B, Caliò I, Lourenço PB. Seismic safety evaluation of reinforced concrete masonry infilled frames using macro modelling approach, Bull. Earthquake Eng. 2017, 15(9): 3871-3895.2017.

Pantò B, Cannizzaro F, Caliò I, Lourenço PB. Numerical and experimental validation of a 3D macro-model for the in-plane and out-of-lane behaviour of unreinforced masonry walls, International Journal of Architectural Heritage 2017, 11(7): 946,964.

Pantò B, Caliò I, Lourenço PB. A 3D discrete macro-element for modelling the out-of-plane behaviour of Infilled Frame Structures, Engineering Structures 2018 (Under Review).

Ricci P, Di Domenico M, Verderame GM. Experimental assessment of the in-plane/out-of-plane interaction in unreinforced masonry infill walls. Eng Struct 2018, 173, 960-78.

Singh H, Paul DK, Sastry VV. Inelastic dynamic response of reinforced concrete infilled frame. Comput Struct 1998;69:685–93.

Taucer F, Spacone E, Filippou FC, A Fiber Beam-Column Element for Seismic Response Analysis of Reinforced Concrete Structures. Report No. UCB/EERC-91/17, 1991, Earthquake Engineering Research Center, College of Engineering, University of California, Berkeley.

Tu Y-H, Chuang T-H, Liu P-M, Yang Y-S. Out-of-plane shaking table tests on unreinforced masonry panels in RC frames. Engineering Structures 32, 2010, p. 3925-335.